Computer Derived Focal Mechanisms for Selected Earthquakes off the South and West Coasts of Turkey

by

T. Hakan Hazneci

Thesis submitted to the Graduate Faculty of
Virginia Polytechnic Institute and State University
in partial fulfillment of the requirements of the degree of

MASTER OF SCIENCE

in

Geophysics

APPROVED:

G. A. Bollinger, Chairman

J. A. Snoke

E. S. Robinson

December, 1983

Blacksburg, Virginia

ACKNOWLEDGMENTS

I would like to thank to Dr. Bollinger for his valuable advice and supervision during the research and completion of this work. I would also like to thank to Drs Snoke and Robinson who critically reviewed the manuscript and made worthwhile comments and suggestions.

I am indebted to Dr. McKeon for his generous help in editing part of the text. Special thanks are also extended to Matthew Sibol and Jeffrey Munsey for their review of the text.

Many thanks are due to Dr. Ergin at the Technical University of Istanbul in Turkey who provided some papers and catalogs.

I would also like to extend my special thanks and appreciation to my parents for their moral support.

TABLE OF CONTENTS

LIST OF FIGURES

LIST OF TABLES

1. INTRODUCTION

The eastern Mediterranean region, bounded by 20 E to 45 E meridians and 30 N to 42 N parallels, lies inside the Alpine-Himalayan orogenic belt system (figure 1). The tectonics and the geology of the region are very complex, and the seismic activity in the region is very intense. Historical data indicate that destructive earthquakes have occurred throughout the past two thousand years up to end including the present (Ambraseys,1970). The seismicity is concentrated along the plate margins and is correlated with major tectonic features (figure 2).

The tectonics of the region have been explained in terms of tectonic models. Models explaining the regional tectonics were introduced by McKenzie (1972), Alptekin (1973), Papazachos (1976), and Dewey and Sengor (1979). These models usually consist of small plates, such as the Turkish and Aegean plates among the much larger, principal plates, the Eurasian, African and Arabian plates. The collision of the Arabian and Eurasian plates in eastern Turkey, causing the westward movement of the Turkish plate, dominates the tectonics of the region. Figure 3 shows the McKenzie (1972) model.

Major tectonic features of the region can be identified as the right-lateral strike-slip North Anatolian Fault, the Bitlis suture zone in eastern Turkey, the left-lateral strike-slip East Anatolian Fault, the east-west oriented graben systems associated with normal faults in western Turkey and the northern Aegean, and the Cretan Arc, where the African plate underthrusts the Aegean plate (figure 1).

The historical earthquakes from AD 11 to the nineteenth century and the earthquakes of the modern instrumental period were compiled by Ergin and others, (1967). Earthquakes with shallow focal depths (60 km and less) occurred through the North Anatolian Fault zone, in western Turkey and in the northern Aegean (figure 2). Earthquakes having intermediate focal depths (greater than 60 km) have been observed in the north of the Cretan Arc, and in the Gulf of Antalya and the Gulf of Iskenderun basins (figure 4). However, events with shallow foci occurred in the south and southwest of Cyprus.

The tectonics of the region have been investigated by employing focal mechanisms of earthquakes occurring in the region by McKenzie (1972) and others. Their focal mechanism solutions were based on P-wave polarity data.

Figure 1 : The tectonic features, the countries and some areas in and around the Eastern Mediterranean. The tectonic features: NA = North Anatolian Fault, EA = East Anatolian Fault, BS = Bitlis suture zone, PMC = Pontid Minor Caucaus zone, KZ = Khoura zone, WTGS = Western Turkey graben system, CA = Cretan Arc, HT = Hellenic Through, MR = Mediterranean Ridge. The countries: USSR = Soviet Union, IR = Iran, IQ = Iraq, SY = Syria, L = Lebanon, CY = Cyprus, JN = Jordan, IS = Israel, EG = Egypt, LB = Libya, GR = Greece, BUL = Bulgaria, ROM = Romania. The areas mentioned in the text: MS = Marmara Sea, GS = Gulf of Saros, R = Rhodes, B = Burdur, FZ = Fethiye zone, GA = Gulf of Antalya, MP = Mut plate, AIB = Adana Iskenderun Basin, GI = Gulf of Iskenderun.

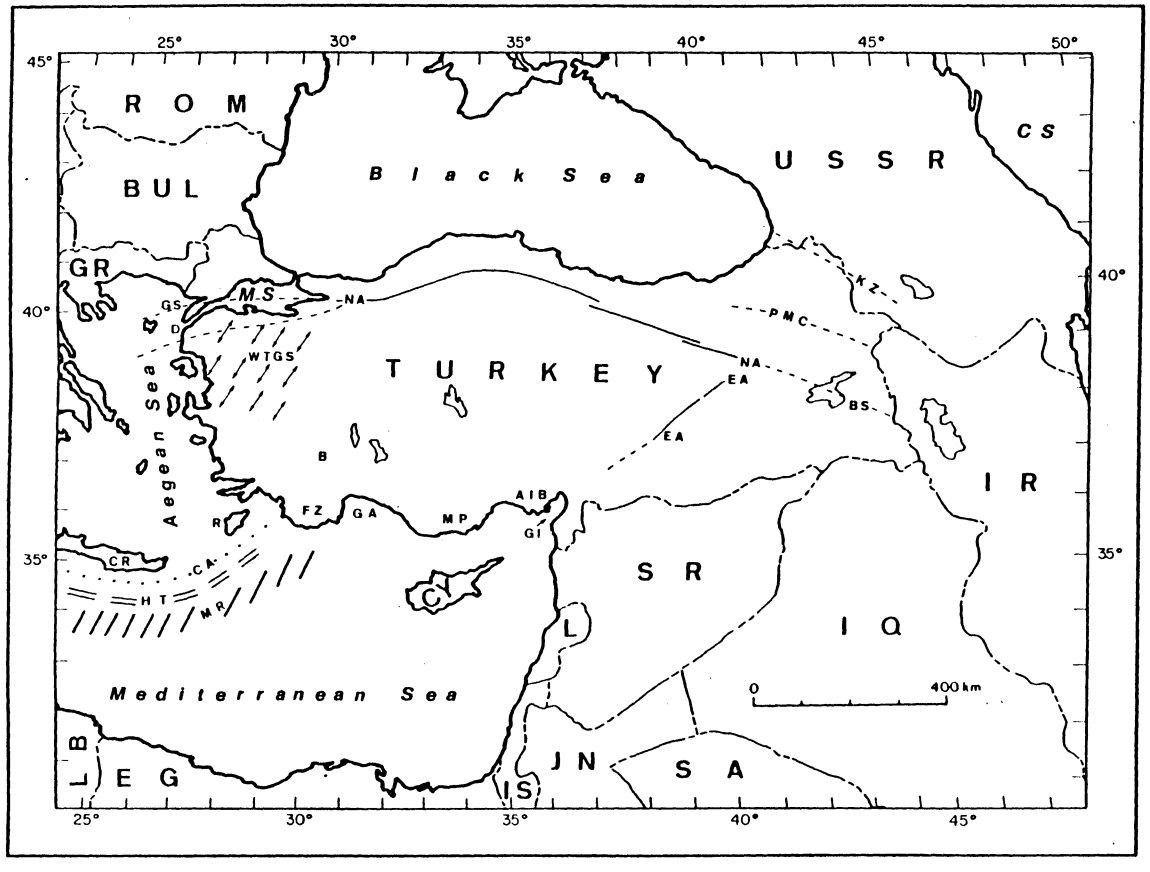
25°
30°
35°
40°
45°
50°
45°
40°
35°
ROM
BUL
GR
Black Sea
USSR
CS
TURKEY
Aegean Sea
Mediterranean Sea
IR
SR
IQ
JN
SA
LEG
IS
CY
MS
NA
EA
PMC
WTGS
FZ
GA
MP
AIB
GI
CR
HT
BS
0
400 km

Figure 2 : Major shallow earthquakes in and around Turkey between AD 11 and 1964. Filled circles represent instrumental epicenters with known focal depths ($h < 60$ km); empty circles show microseismic epicenters with no depth information. Adapted from Ergin, et al., (1967).

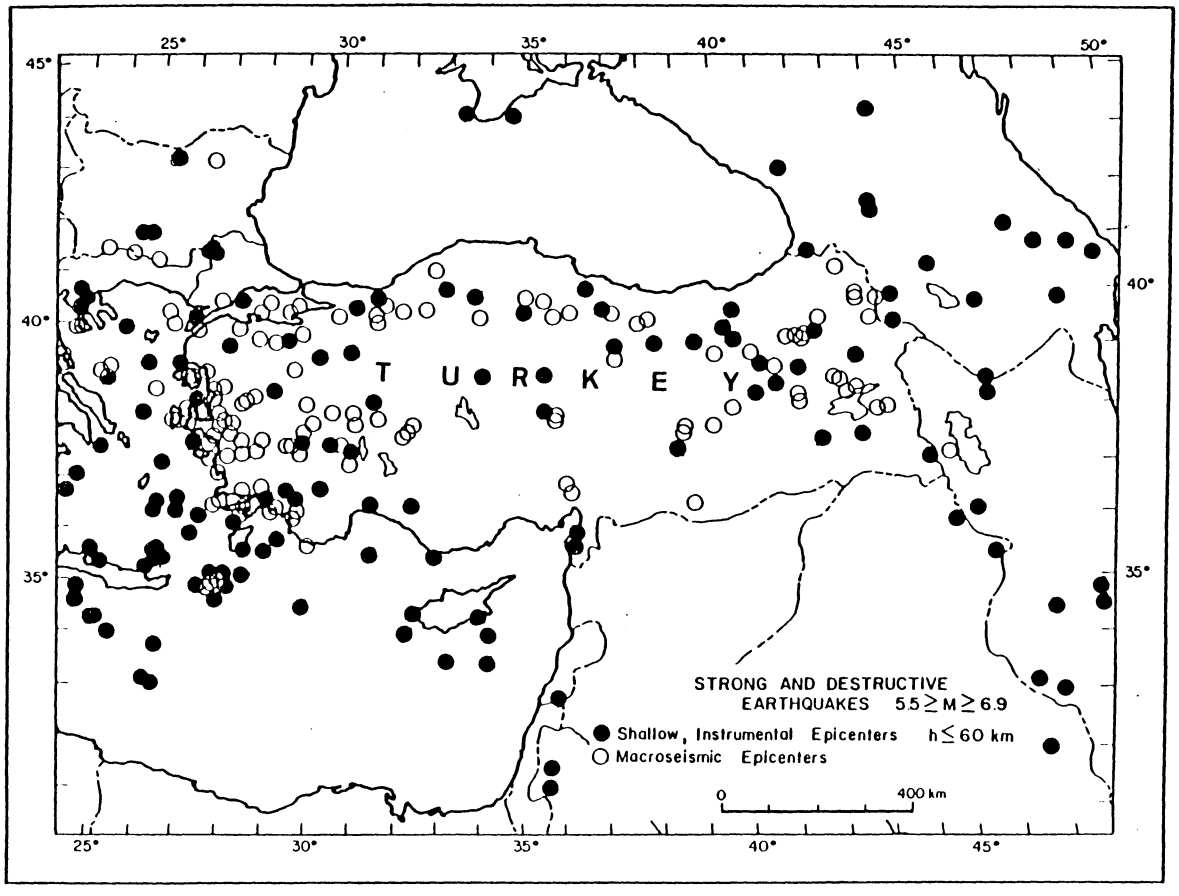
25°
30°
35°
40°
45°
50°
45°
40°
35°
T U R K E Y
STRONG AND DESTRUCTIVE
EARTHQUAKES 5.5 ≥ M ≥ 6.9
Shallow, Instrumental Epicenters h ≤ 60 km
Macroseismic Epicenters
0
400 km

Figure 3 : Plate boundaries and relative velocities. Arrows show the direction of motions. Length of arrows are proportional to the magnitude of the velocity. Heavy lines transform faults, crossed lines are boundaries where underthrusting is taking place. Double lines are also plate boundaries. Plates; 1 Eurasian, 2 African, 3 Iranian, 4 South Caspian, 5 Turkish, 6 Aegean, 7 Black Sea, and 8 Arabian. Adapted from McKenzie (1972).

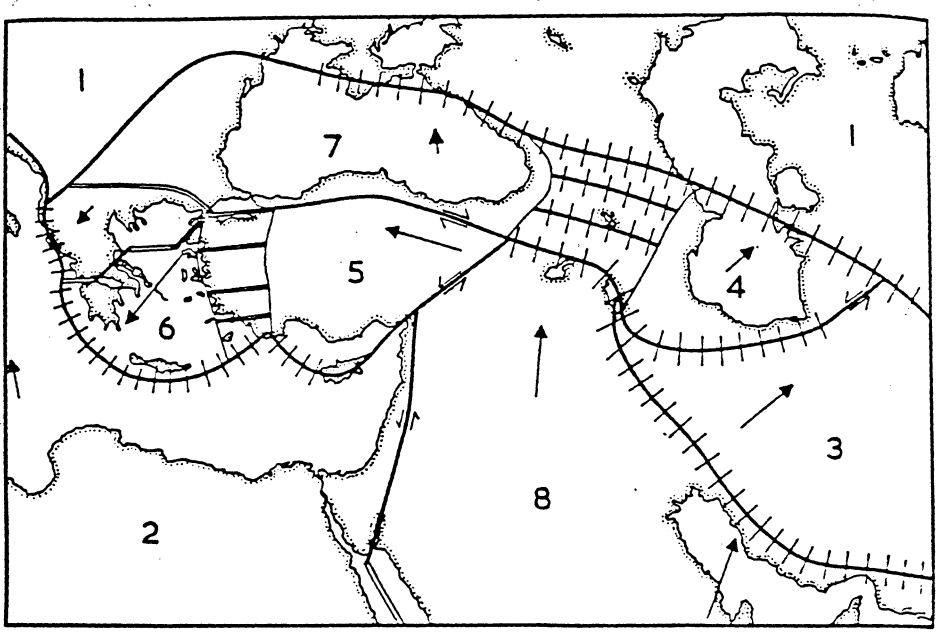
1
7
1
5
4
6
3
8
2

Figure 4 : Deep or intermediate earthquakes in the eastern Mediterranean region between AD 11 and 1964. Adapted from Ergin, et al., (1967).

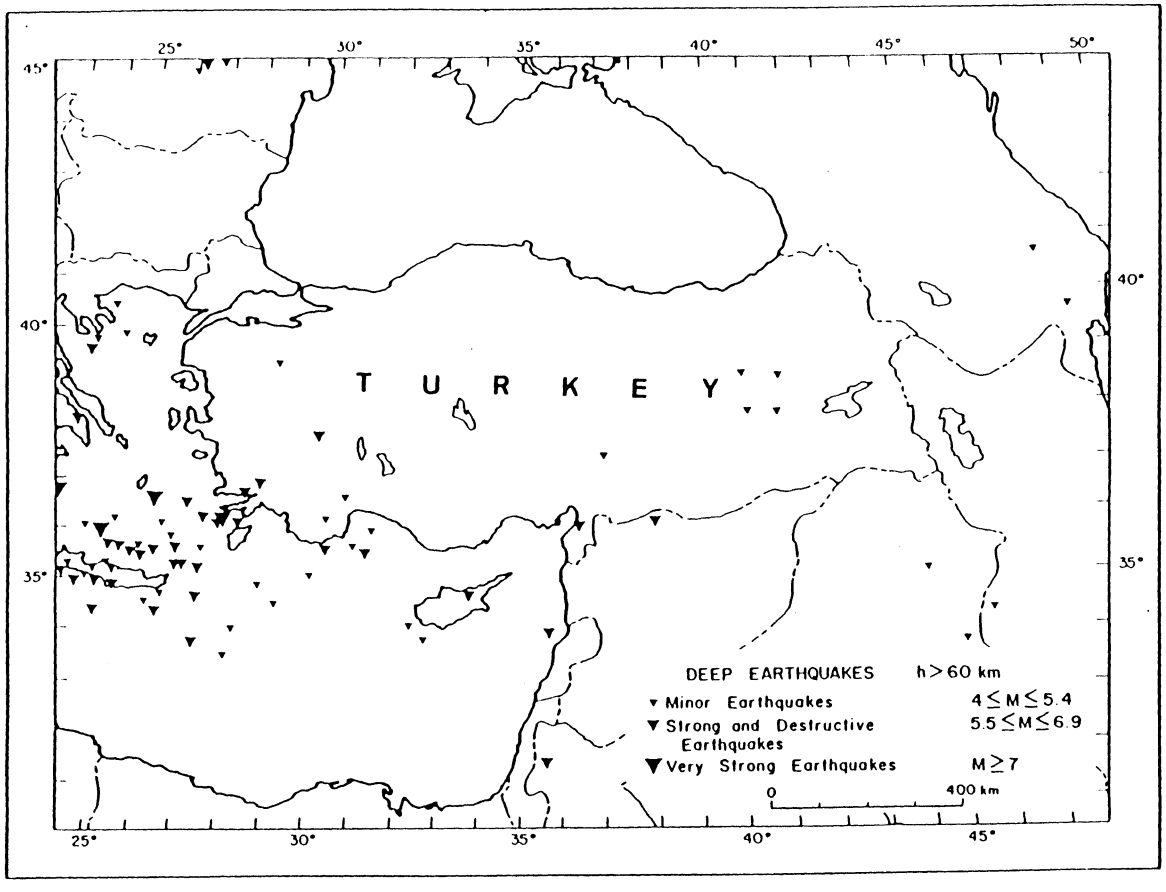
25°
30°
35°
40°
45°
50°
45°
40°
35°
T U R K E Y
DEEP EARTHQUAKES h>60 km
Minor Earthquakes 4≤M≤5.4
Strong and Destructive Earthquakes 5.5≤M≤6.9
Very Strong Earthquakes M≥7
0
400 km

In this study, focal mechanisms of three of the four earthquakes (1 June 1977 and 28 May 1979 events in the Gulf of Antalya, 14 June 1979 event in the Aegean Sea) were determined using both P-wave polarities and S-wave polarization angles. Additionally, a P-wave polarity data only focal mechanism solution was determined for a fourth earthquake (26 April 1981 event in the Gulf of Antalya).

The seismograms for these shocks were obtained from the World Wide Standard Seismograph Network (WWSSN) stations. Additional P-wave polarity data were obtained from published listings (U.S. Geological Survey's Earthquake Data Reports (EDR)). The S-wave polarization angles were determined directly from the S-wave particle motion diagrams constracted for the stations having epicentral distances greater than 44 degrees. A technique developed by Nuttli (1964) was also applied to determine the polarization angles from particle motion plots for the stations with the epicentral distances less than 44 degrees, for which the S-wave particle motion at the free surface is not linear with respect to vertical and horizontal components.

A computer program, originally written by Guinn (1977) was utilized to obtain focal mechanism solutions for these earthquakes. Preferred and alternative solutions were obtained.

2. OVERVIEW OF THE SEISMOTECTONICS AND THE GEOLOGY IN THE EASTERN MEDITERRANEAN

The Eastern Mediterranean region lies inside the Alpine-Himalayan orogenic system. The collision of Africa and Eurasia caused Alpine orogeny, whereas the collision of Asia and India produced the Himalayan orogeny. The tectonics and the geology of the region are complicated because several small minor plates, including the Turkish and the Aegean, exist between the major plates, the Eurasian the African and the Arabian (McKenzie, 1972). The distribution of seismicity in the region is not homogeneous. Much of the seismicity concentrates along the plate boundaries. Figures 2, 4 and 5 show the epicentral distribution of major earthquakes in the Aegean Sea and the Eastern Mediterranean and Turkey (Ergin, et al., 1967). Beginning with Turkey, the seismotectonics and the geology of the region will now be described.

2.1 Turkey

Turkey is a principal part in the Mediterranean sector in the Alpine-Himalayan orogenic belt system. The seismotectonics of the region have been explained in terms of global plate tectonics (McKenzie, 1972 Alptekin, 1973

Figure 5 : Very strong earthquakes (M > 7.0) in the eastern Mediterranean region between AD 11 and 1964. Filled circles stand for instrumentally located shallow earthquakes (h < 60 km) whereas empty circles stand for the earthquakes with unknown focal depths. Adapted from Ergin, et al., (1967).

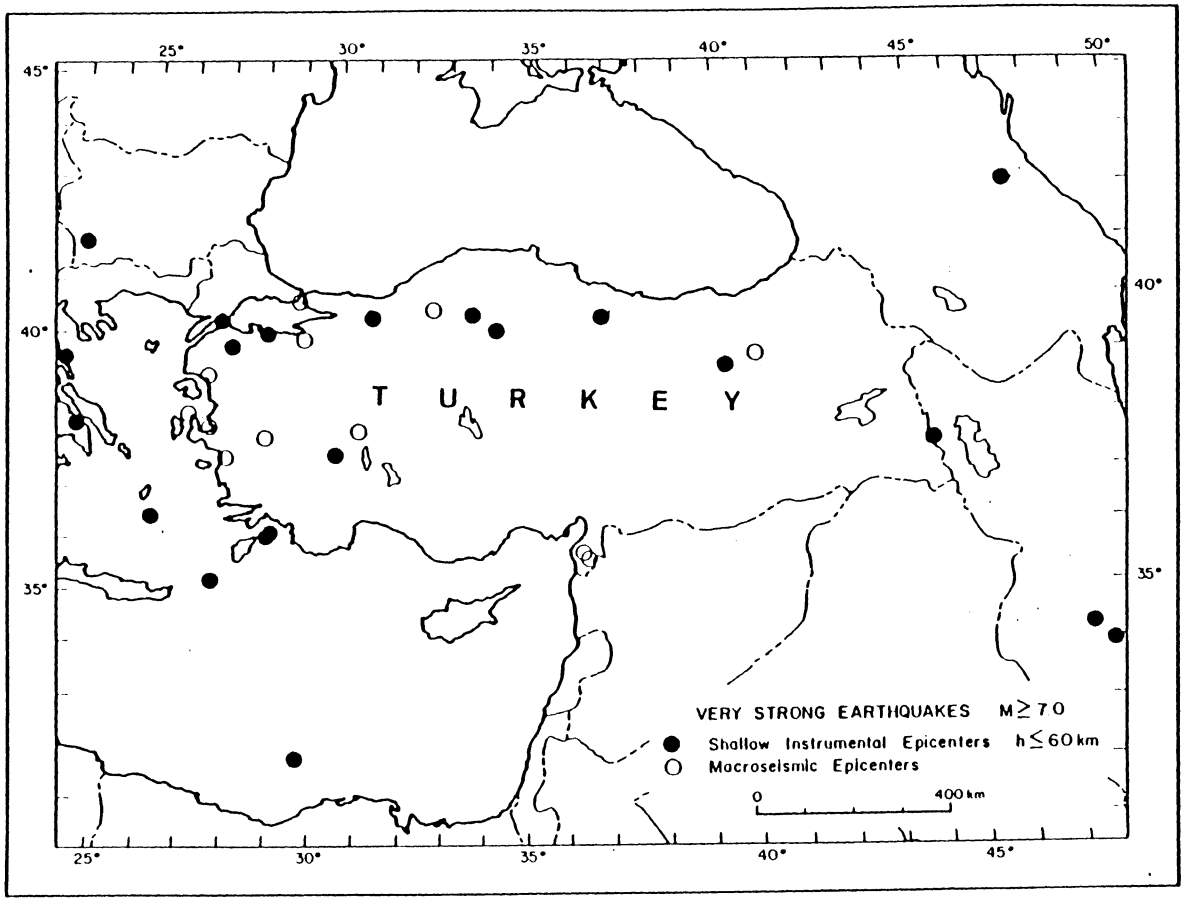
25°
30°
35°
40°
45°
50°
45°
40°
35°
T U R K E Y
VERY STRONG EARTHQUAKES M≥7.0
Shallow Instrumental Epicenters h≤60 km
Macroseismic Epicenters
0
400 km

Papazachos, 1976 Dewey and Sengor, 1979). The model introduced by McKenzie (1972) for the eastern Mediterranean region consists of eight plates, including the three principal plates: the Eurasian, African and Arabian. Figure 3 shows a sketch of these plate boundaries and relative plate velocities.

The North Anatolian Fault constitutes the boundary between the Turkish and the Black Sea plates, whereas the East Anatolian Fault constitutes the boundary between the Turkish and the Arabian plates. The Turkish plate is squeezed together by the collision of the Eurasian and the Arabian plates east of the intersection of the North Anatolian and the East Anatolian faults. As a result of this collision, the Turkish plate moves westward rapidly resulting a right-lateral motion along the North Anatolian Fault and a left-lateral motion along the East Anatolian Fault (McKenzie,1972 Alptekin,1973 Dewey,1976 Dewey and Sengor,1979). The collision zone was identified as the Bitlis suture zone in the southeastern Turkey and as Pontide/minor Caucasus and Khoura zones in northeastern Turkey (Dewey and Sengor,1979). The strike-slip character of the North Anatolian Fault changes to strike-slip and overthrust in the collision zone (McKenzie,1972).

The North Anatolian Fault is longer than 800 kilometers and well-defined surficially in its east portions. In the west part, the termination of the fault is not well-known. The recent estimates of that termination range from 30.5E (McKenzie,1972) to 28.5E degrees (Ambraseys,1970). Many sections of the fault are active and seven earthquakes with magnitudes of 6.8 to 8.0 ruptured along the North Anatolian Fault from 1939 to 1967 (Dewey,1976) (figure 5). A Quaternary age for the age of the fault was suggested by Ketin (1969). However, Pavioni (1961) argued that the fault had been present in a much earlier period and that its movement involves a total lateral displacements of several hundred kilometers (Ketin (1969), Pavioni (1961) in Ambraseys (1970)). According to Ambraseys (1970), the recent fault zones were observed to be almost 1-2 kilometers wide and many surface breaks could be observed. He also added that the displacement of the fault from 1939 to 1967 was 90 centimeters. Annual displacements of the fault have varied from three to twelve centimeters (Toksoz, Shakal and Michael,1979).

Surface breaks of many large earthquakes occurring along the North Anatolian Fault zone indicated shallow foci (Dewey,1976). Moreover, Canitez and Toksoz (1971), using Love/Rayleigh spectral ratios, have estimated focal depths

of ten to twenty kilometers for the large earthquakes occurring in North Anatolia. The detailed nature of the shallow focal depth distribution is not known at present.

In northwestern Turkey, the strike slip character of the North Anatolian Fault changes to a series of normal faults with east-west trends in two strands. The northern strand crosses the Marmara Sea Basin. The southern strand passes the region south of the Marmara Sea. Alptekin (1973) considered the southern strand active. Nevertheless, Dewey and Sengor (1979) suggested both strands are active up to their termination in the northern Aegean Sea.

The East Anatolian Fault is considered inactive compared to the North Anatolian Fault (McKenzie,1972). However, according to Ambraseys (1970), large shocks have occurred in the East Anatolian Fault sporadically during the past two thousand years. Currently, the nature of this fault is not well understood. The East Anatolian Fault extends in a southwest direction toward the Gulf of Iskenderun. Allen (1969, in McKenzie (1972)) favores the continuation of the East Anatolian Fault to the Dead Sea Rift through Syria and Lebanon. However, McKenzie (1972) contends that the fault continues on in a large loop from the Gulf of Iskenderun through the south of Cyprus to Rhodes (figure 3).

In western Turkey, east-west oriented graben zones associated with normal faults are considered the major seismically active zones. These zones constitute the boundary between the Turkish and the Aegean plates (McKenzie,1972).

The geologic structures in Turkey were formed during and the post Alpine-Himalayan orogenic period. Orogenic developments in the post orogenic period were very intense; associated block faulting has modified the topography. Several grabens parallel to the Alpine-Himalayan belt system were formed then. The Aegean and the Marmara Sea basins were also formed during the post orogenic period (Ilhan (1971) in Alptekin (1973)). The structures defined by Ketin (1968) were (1) metamorphic-crystalline massifs, (2) folded paleozoic mountain chains, (3) major faults and overthrusts of the late Alpine period, (4) grabens and depressions of the post Alpine period, (5) active faults, and (6) major earthquake zones (Ketin (1968) in Alptekin (1973)).

Metamorphic-crystalline massifs were observed in western, central and in southeastern Anatolia. They consist of mafic and silicic crystalline rocks. Some massifs having Paleozoic age were formed during the Caledonian and Hercynian orogenies. Other massifs having lower Mesozoic

age were formed during the beginning stages of the Alpine orogeny.

Folded Paleozoic mountain chains developed around the Marmara Sea Basin in northwestern Anatolia. However, the youngest mountains of the Alpine orogeny having the Mesozoic-Tertiary age were formed at the Black Sea coastal mountains and Taurus mountains of the Mediterranean coast of Turkey.

2.2 The Aegean Sea

The tectonics of the region is complicated due to the rapid westward movement of the Turkish plate. The Aegean plate, defined by McKenzie (1972) consists of part of Greece, part of the Aegean Sea, Crete and part of Turkey (figure 3). McKenzie introduced another plate in northern Greece without naming it. The boundaries of the Aegean have evolved since late Miocene (Dewey and Sengor,1979). The Greek-Aegean boundary, a ridge transform system runs from the Dardanelles to the Gulf of Corinth (figure 5). The Turkish-Aegean boundary is defined by east-west oriented graben systems. The African-Aegean boundary, the Cretan Arc, extends from west of the Gulf of Corinth through the south of Crete to southwestern Turkey. The total length of the Cretan Arc is estimated to be 1500 kilometers (figure 6).

Alptekin (1973) considered the Turkish and the Aegean plates together and called them the Aegean-Turkish plate because of the poorly defined boundary in western Turkey. However, the widespread seismicity around the Aegean supports the existence of these two plates (McKenzie,1972). Additionally, Dewey and Sengor (1979) suggested another model for the Aegean tectonics. They proposed a Paleponnesian plate in the central Aegean and the Cretan plate in the southern Aegean. Nevertheless, McKenzie's and Dewey and Sengor's plate tectonics models seem to agree in the northern Aegean. The plate without a name assigned by McKenzie was later called 'the Macedonian plate' by Dewey and Sengor (1979).

The fault plane solutions obtained by McKenzie (1972), Alptekin (1973) and Papazachos (1976) show that all types of faulting has occurred in the Aegean. However, normal faulting has dominated and associated with the grabens in northeastern Aegean (figure 6).

The fault movements along the Cretan Arc, the southern boundary of the Aegean plate are very well-determined by the focal mechanism solutions (McKenzie,1972). Most of the solutions show low angle thrusting with little or no strike-slip component. McKenzie interpreted the northward dipping planes of the mechanisms as fault planes because of

Figure 6 : A: Simple configuration of the Aegean tectonics showing the regions of compression, extension and strike-slip inferred from focal mechanisms obtained by McKenzie (1972), Alptekin (1973), and Papazachos (1976). B: The focal mechanism solutions of the Aegean earthquakes plotted on an Aegean map. White = dilatational quadrants; black = compressional quadrants; stippled areas = Neogene-Quaternary grabens; empty circles = hot springs; heavy lines (broken where poorly defined) = faults; heavy lines with empty triangles on upper plate = subduction zone. Adapted from Dewey and Sengor (1979).

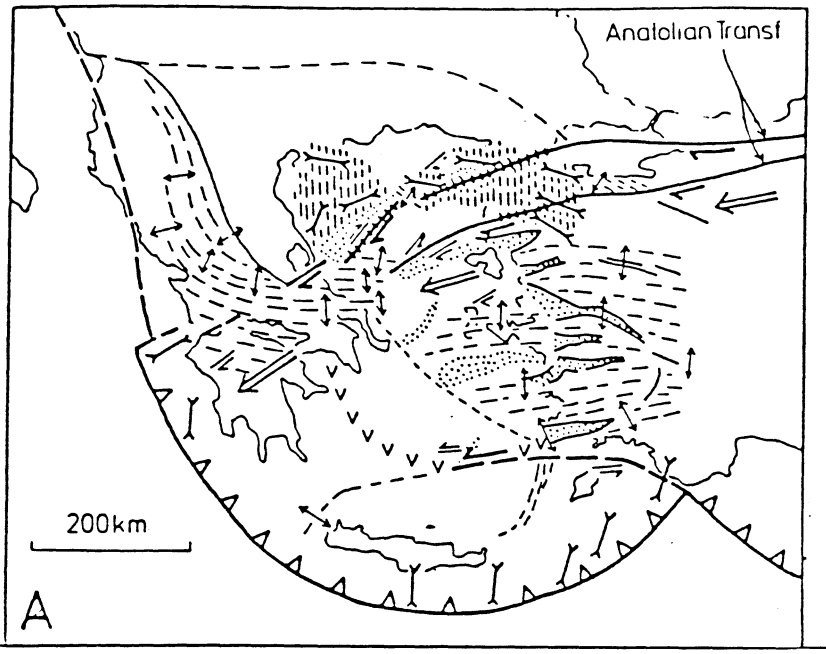
Anatolian Transf
200km
A

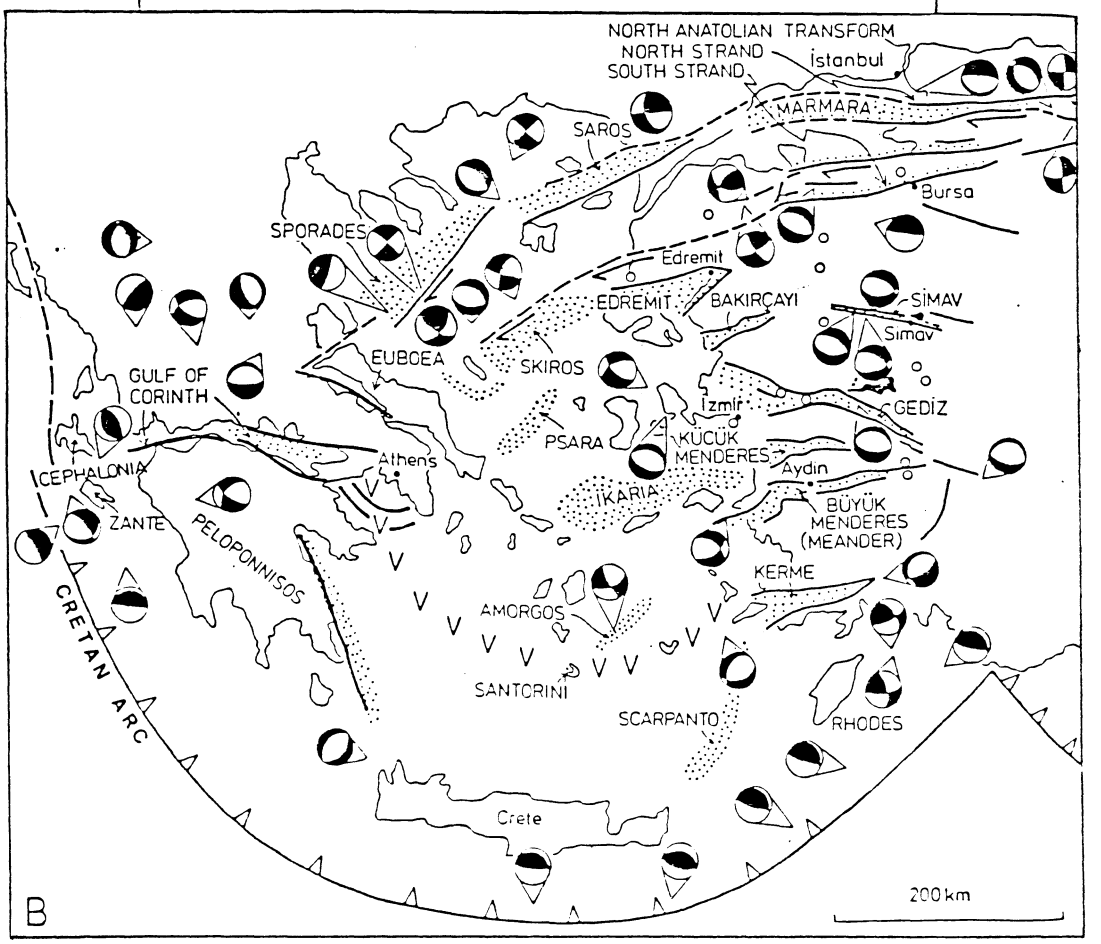
NORTH ANATOLIAN TRANSFORM
NORTH STRAND
SOUTH STRAND
İstanbul
MARMARA
SAROS
Bursa
SPORADES
Edremit
EDREMIT
BAKIRÇAYI
SİMAV
Simav
EUBOEA
SKIROS
GULF OF CORINTH
İzmir
GEDİZ
PSARA
KÜÇÜK MENDERES
Aydin
CEPHALONIA
Athen's
İKARIA
BÜYÜK MENDERES (MEANDER)
ZANTE
PELOPONNISOS
KERME
AMORGOS
CRETAN ARC
SANTORINI
SCARPANTO
RHODES
Crete
200km
B

the deeper seismic activity to the north of the Cretan Arc and the observation of volcanic activity in the central Aegean.

The other two boundaries of the Aegean plate were poorly determined due to the scattered seismic activity and the lack of continuation of tectonic structures. Most shocks in the mainland of Greece, Albania and southern Yugoslavia are associated with normal faulting (figure 6). However, none of these shocks produced surface breaks. The eastern boundary was defined with graben systems in a region of 400 kilometers wide from the Gulf of Saros to Rhodes. In this broad region, all the fault plane solutions showed normal faulting except the Burdur earthquake on 12 May 1971, which had a mechanism of right-lateral srike-slip faulting indicating an arc-to-arc transform fault in the eastern end of the Cretan Arc (Alptekin,1973).

2.3 The Eastern Mediterranean Sea

The tectonic evolution of the region started much earlier than the late Miocene collision of the African and Eurasian plates that produced the Alpine orogeny. Earlier, the Mediterranean Sea was thought to be the remains of the Tethys Ocean existing between Africa and Eurasia during the Cretaceous and early Tertiary times (Alptekin,1973).

Nevertheless, some geologists believe that most of the present Mediterranean crust formed with a newly oceanized continental crust (Gilluly,1972 in Alptekin,1973).

Prior to the late Miocene, a phase of crustal extension and rifting occurred in the eastern Mediterranean. Then, in late Miocene collision, the extensional phase changed to a compressional phase (Ryan, et al., 1970 in Alptekin, 1973), producing the underthrust of the African plate beneath the Aegean and Turkish plates. The physical features of the Mediterranean seabed record the existence of these two phases. The Mediterranean Ridge extends from the southwest of Greece through the south of the Cretan Arc to the southeast of Rhodes. The region between the Mediterranean Ridge and the Cretan Arc having an approximate length of 1500 kilometers was called the Hellenic Through (figure 1) (Alptekin,1973).

McKenzie (1972) suggested a plate boundary between the Turkish and African plates, extending from the Gulf of Iskenderun through the south of Cyprus to Rhodes exhibiting the continuous seismic activity along the boundary. He considered this boundary as a continuation of the East Anatolian Fault (figure 3). McKenzie believed the slip rate on the East Anatolian Fault to be too rapid to be taken up by the Dead Sea Rift system introduced by Allen (Allen (1969) in McKenzie (1972)).

Figure 7 : Epicentral distribution of major earthquakes between 1903 and 1976 in the eastern Mediterranean Sea and southern Turkey. Adapted from Ergin and Buyukasikoglu, (1978).

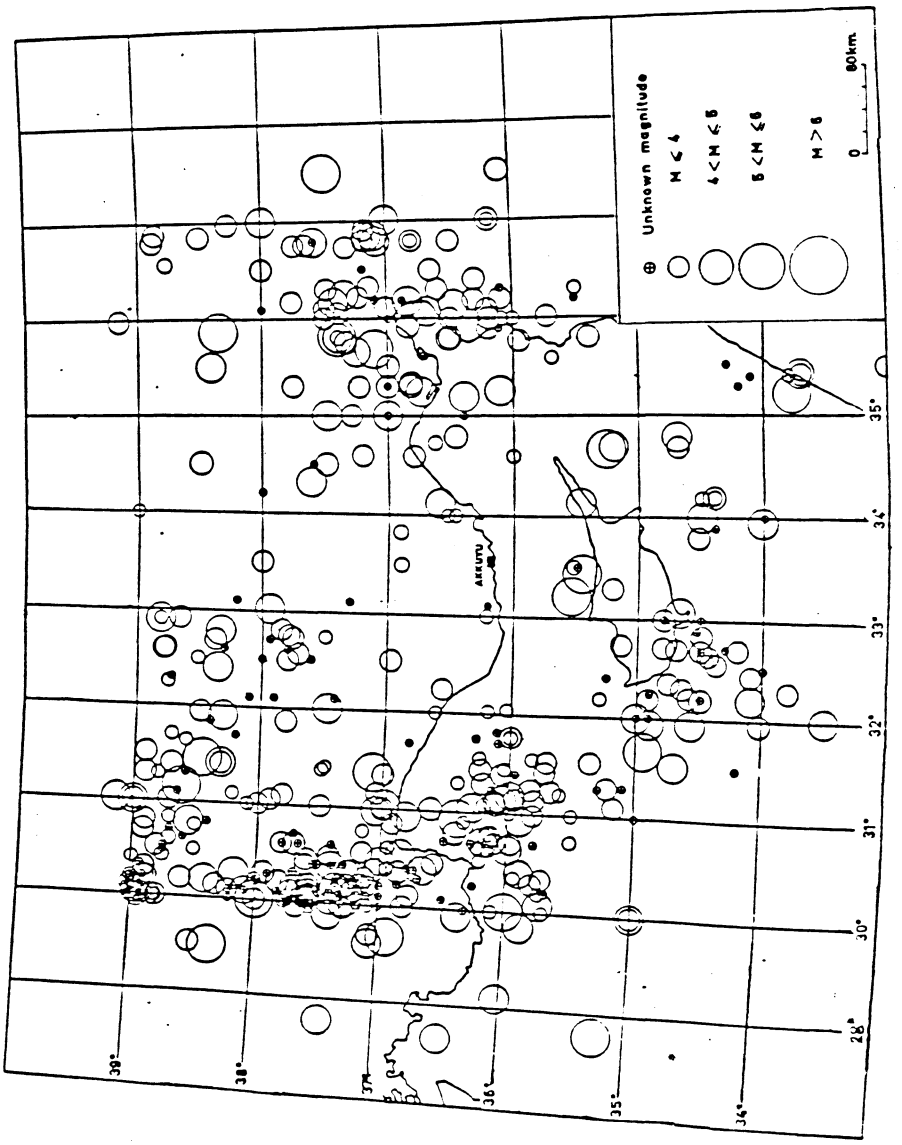
Unknown magnitude
M ≤ 4
4 < M ≤ 5
5 < M ≤ 6
M > 6
0
80km
ANKARA
39°
38°
37°
36°
35°
34°
35°
34°
33°
32°
31°
30°
28°

Figure 8 : Epicentral distribution of the eastern Mediterranean Sea earthquakes between 1903 and 1976 based on their classification with respect to focal depths. Adapted from Ergin and Buyukasikoglu (1978).

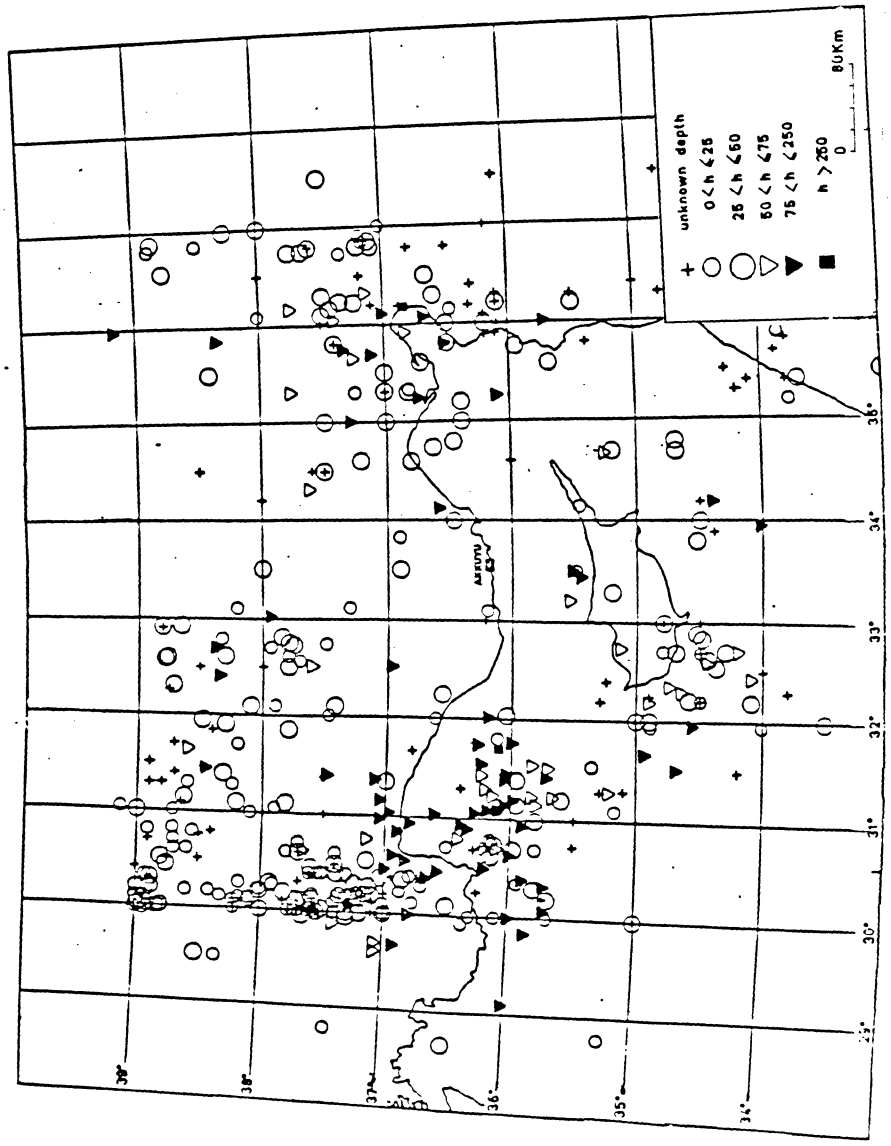
unknown depth
0 < h ≤ 25
25 < h ≤ 50
50 < h ≤ 75
75 < h ≤ 250
h > 250
0
80Km
ARAVA
38°
37°
36°
35°
34°
33°
32°
31°
30°
29°

The seismicity of the region has been studied extensively by Ergin and Buyukasikoglu (1978), covering the destructive earthquakes of the eighteenth and nineteenth centuries as well as the earthquakes of the instrumental period from 1901-1976 (figures 7 and 8). The distribution of seismicity showed the following; (1) shallow earthquakes in the Turkish mainland and offshore areas; (2) the earthquakes with intermediate focal depths ($60 < h < 250$ km) in the Gulf of Antalya, and the Gulf of Iskenderun and Adana basins (figure 8); (3) the earthquakes with shallow and intermediate depths in the south and southwest of Cyprus; (4) An aseismic zone called the Mut platform in Harsch and Kuepfer (1980) in the Turkish mainland between the Antalya and Adana-Iskenderun basins (figure 1).

3. THE METHODS USED FOR THE DETERMINATION OF FOCAL MECHANISMS

In this chapter, the collection and analysis of P and S-wave data and the computer focal mechanism determination techniques are discussed. Then, preferred and alternative solutions for one Aegean Sea and three Gulf of Antalya earthquakes are presented.

3.1 Collection and Analysis of P and S Data

The majority of data consists of P-wave polarities obtained from long period, vertical (LPZ) records of Worldwide Standard Seismograph Network (WWSSN) stations. In a few instances, polarities were also obtained from short period vertical (SPZ) records when the long period vertical (LPZ) records were not available. Reported polarities in USGS Earthquake Data Reports (EDR) for stations other than WWSSN and for some WWSSN stations for which seismograms were not available, were also employed in focal mechanism determination.

S-wave polarization angles were determined by means of particle motion diagrams. Only for stations with epicentral distances greater than 44 degrees is the ground motion linear and related directly to the incident motion. At

smaller distances, the S-wave particle motion at the free surface is non-linear with respect to the vertical and horizontal components due to a phase shift in vertical component which consists of incident SV, reflected SV and a reflected imaginary P-wave phase. However, Nuttli developed a technique for polarization angle determination in the non-linear range. In his analysis procedure, Nuttli considered four different crustal models; (1) an average continental crust, (2) the crust beneath the central United States, (3) a thick crust and (4) a thin crust so as to allow for a wide variety of possible receiver crustal structures.

Nuttli (1964) derived the following equations for the polarization angle (epsilon) in the non-linear range:

$$\text{Tan}(\text{epsilon}) = \text{Fh} * \text{Tan}(\text{gamma})$$

$$\text{Tan}(\text{epsilon}) = \text{Fv} * \text{Tan}(\text{delta})$$

where gamma is the angle between the horizontal component of the S-wave particle motion and the great circle path at the station, and delta is the angle between the vertical axis and the component of the S-wave particle motion in the plane transverse to the great circle path (Nuttli,1964).

Fh and Fv are functions of the wave period, epicentral distance, and crustal structure beneath the recording station. Figure 9 shows how gamma and delta are defined.

The radial and horizontal components of S-wave surface motion (UR and UH, respectively) are computed as follows:

$$UR = UN * Cos(Ase) + UE * Sin(Ase)$$

$$UH = UN * Sin(Ase) - UE * Cos(Ase)$$

where UN and UE are the horizontal components of particle motion in the directions of north-south and east-west respectively. Ase is the azimuth of the great circle path at the station towards the epicenter (also called the back azimuth).

Gamma and delta angles using plots of S-wave surface motion and both Fh and Fv values for an average worldwide crustal model were determined for ten stations in order to compare polarization angles obtained by using the different components of the particle motion. Table 1 shows those polarization angle values for the Aegean earthquake of 14 June 1979.

Figure 9 : Particle motion diagram sketches giving the definition of gamma and delta. UR = Radial particle motion; UZ = Vertical particle motion; UH = Horizontal particle motion. Adapted from Nuttli (1964).

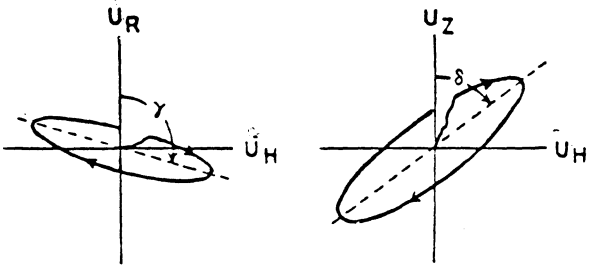
U_R
γ
U_H
U_Z
δ
U_H

Table 1

Comparison and Basis of Selection of the Computed Polarization Angles for the Earthquake of 14 June 1979

Station	E(Fh),deg	E(Fv),deg	Basis for Selection
COP	-7	4*	Largest particle motion Fh changing rapidly
NUR	6	-22*	Most linear particle motion Fh changing rapidly
KON	12	-4*	Largest particle motion Fh changing rapidly
PTO	-19*	13	Most linear particle motion Largest particle motion
VAL	4	2*	Most linear particle motion
KEV	-14*	-3	Most linear particle motion
AAE	31*	5	Largest Particle motion
KTG	-19	4*	Most linear particle motion Fh changing rapidly
NAI	61*	-17	Most linear particle motion Fv changing rapidly
NDI	-46*	-23	Fv changing rapidly

* : Indicates epsilon (E) was chosen as the most appropriate value. The average difference between the two determinations of polarization angles for ten stations is 25 degrees. The standard deviation of the average difference is 33.6 degrees. These values indicate that the S-wave surface motion is mixed with some noise and/or another phase.

Fh and Fv values were determined from the charts of S-wave period versus epicentral distance (Nuttli,1964). The Fh and Fv values change rapidly for certain epicentral distances and certain periods of S waves. Thus, to avoid errors in the calculation of the S-wave polarization angles, the slowly changing regions for the values of Fh and/or Fv are preferred. When both Fh and Fv values do not change rapidly, other criteria such as largest particle motion, and/or most linear particle motion were applied to select the most appropriate values of the polarization angles.

3.2 Computer Determination of Focal Mechanisms Using P-wave Polarities and S-wave Polarization Angles

The computer program used for this study was written originally by Guinn and Long (Guinn,1977) but was revised to include S-wave polarization angles and the SV to P amplitude ratio. The double-couple source model was adopted for all focal mechanism analyses.

An iterative technique employed in the program, searches the focal sphere for mechanism solutions compatible with the input P-wave polarities and S-wave polarization angles. The P and S data and the B, null

axis, which represents the intersection of the two nodal planes, are defined within a right handed rectangular coordinate system with X1, X2 and X3 axes as north, east, and down, respectively. The polarity data are transformed to a new coordinate system for which the X3 axis coincides with the B-axis. Then the polarity data are rotated around the B-axis and are checked systematically in each quadrant. If the total number of inconsistent first motions is equal to or less than a predefined, allowed number of inconsistent first motions, a solution is declared valid based on P-wave polarity data only. If S-wave data are available, the program also checks them for compatibility. This technique is applied by generating a 5 by 5 grid of 25 B-axes around a central B-axis. After searching the possible solution for each B-axis position, the central B-axis is moved to another location. A grid interval or increment angle of 10 degrees is recommended for an optimal search of the focal sphere.

After checking the polarity data, the program computes the theoretical polarization angles for the given solution and compares them with the observed polarization angles. The number of inconsistent S-wave polarization angles is obtained by designating a maximum difference between the theoretical and the observed polarization angles in

advance. An average difference of 20 degrees was employed because that level of deviation is regarded as representing good empirical agreement between the S-wave data and the focal mechanism solution (Stauder and Bollinger, 1964). When the total number of inconsistent S-wave polarization angles is equal to or less than the predefined number of inconsistent S-wave polarization angles, a solution is declared and the pressure (P), tension (T), and null (B) axes are computed.

In the program, the method of calculating the difference between the theoretical and the observed S-wave polarization angles has been revised slightly by the author. Previously, the theoretical and observed displacement vectors of the S-wave along the X1, X2, X3 axes, (which are in the form of the geographic coordinate axes; north, east, and down) were computed to determine the angular difference between the theoretical and the observed displacements. In the currently used method the theoretical polarization angle is computed directly from the ratio of the horizontal (USH), and the vertical displacements (USV) using Herrmann's (1975) expressions for USH and USV. A subroutine (EPSLN) has been added to the program to calculate the theoretical polarization angles and their differences with the observed ones.

Obviously when P and S data are used together, the focal mechanism solution is better constrained than when only one class of observations are used. To illustrate the advantage of additional constraints, the computer program was run twice for the Gulf of Antalya Earthquake of 1 June 1977. First only P data were used and 11 solutions were obtained. Second, both P and S data were used and only one solution was obtained. Figure 10 shows these results.

3.3 Focal Mechanism Solutions

Tables 2, 3, 4 and 5 show the mechanism results obtained for the four earthquakes studied. These events had magnitudes varying between 5.4 and 5.9. Three of the four events (1 June 1977, 28 May 1979, and 14 June 1979) were studied using both P and S data. However, for the fourth (26 April 1981) only P data were employed because reliable S data could not be obtained. Additionally, three of the four earthquakes were located in the Gulf of Antalya, in the Mediterranean Sea (1 June 1977, 28 May 1979, and 26 April 1981), and one was in the Aegean Sea just off the coast of Turkey (14 June 1979).

The focal mechanism results in the tables 2 through 5 are given as strike, dip, and slip angle of the nodal planes, the trend and plunge of the B, P, and T axes and the trend and plunge of X and Y poles of the nodal planes.

Figure 10 : The lower hemisphere projection of the focal mechanism solution of 1 June 1977 earthquake using only P data and using P and S data together. The higlighted latters of P, T, and B show the focal mechanism solution derived using P and S data together. Number of inconsistencies were 3 for P-wave polarities and 1 for S-wave polarization angles for that solution.

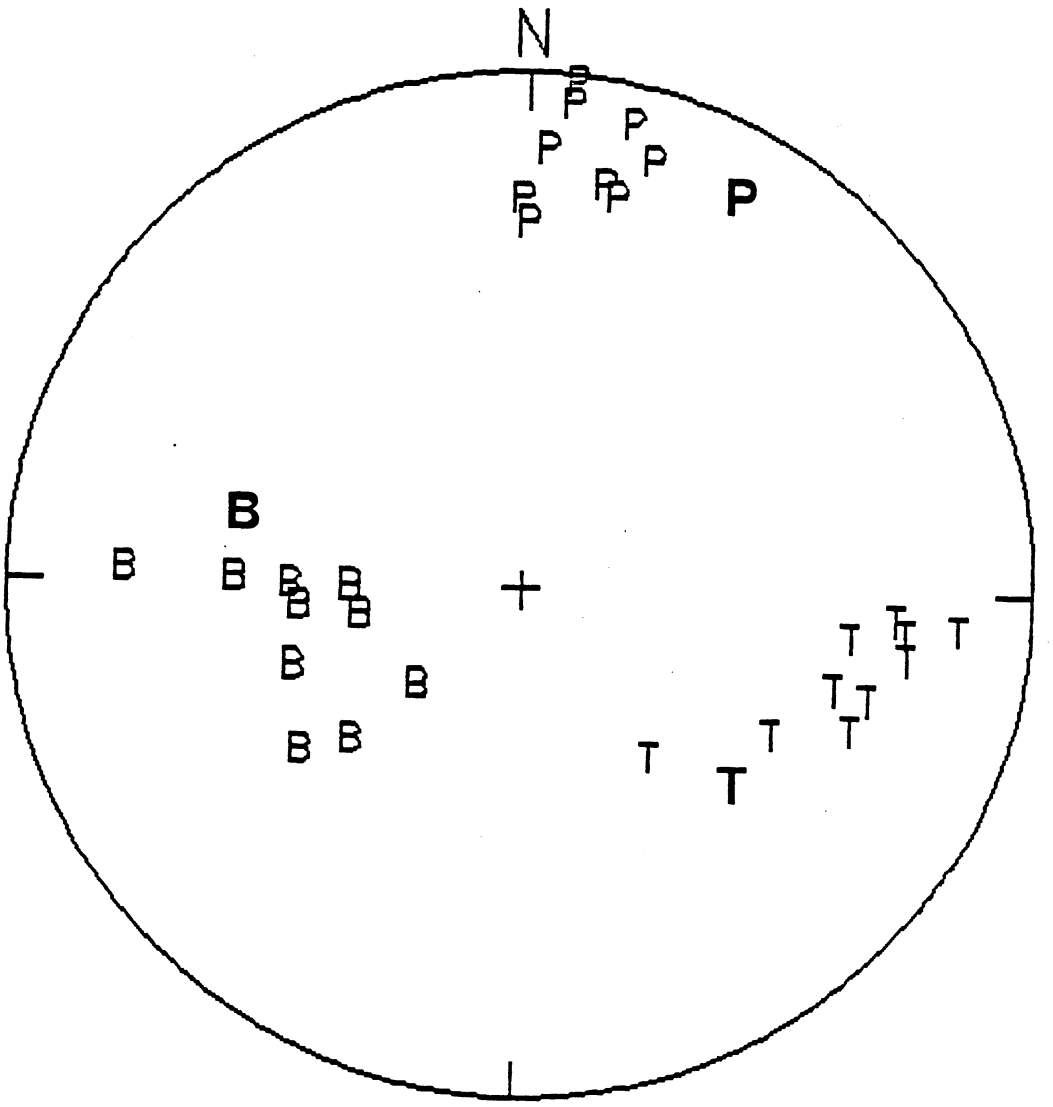
N
P
B
T

The preferred focal mechanism for the four events along with the P- and S-wave data are given in figures (11, 13, 15, and 17). Each of the figures (12, 14, 16, 18) show four alternative solutions for each earthquake. These alternative solutions are obtained by easing the restrictions on the number of inconsistent P-wave polarities and the number of observed S-wave polarization angles which have differences greater than 20 degrees with their theoretical polarization angles. More information about the restrictions of the P and S data are given in the figure captions.

Table 2

Focal Mechanism Solution for The Earthquake of 1 June 1977

Southwestern Turkey 1 June 1977 Origin: 12:54:49.2 UTC

Gulf of Antalya 36.2N-31.34E Depth = 66 Km. Mb = 5.7

Axis	Trend	Plunge	Nodal Planes	Strike	Dip	Slip
P	27	18	plane 1	267	75	47
T	135	43	plane 2	161	45	22
B	281	41				
X	71	45				
Y	177	15				

S-wave Data:

Number of polarization angles = 12

Average error = 10.23 degrees

Standard deviation = 12.01 degrees

P-wave Polarity Data:

3 inconsistencies out of 52 (6%)

Number of WWSSN Station Data: 31

Reference Source of data: USGS Earthquake Data Report (EDR)

Table 3

Focal Mechanism Solution for the Earthquake of 28 May 1979

Southwestern Turkey 28 May 1979 Origin: 09:27:32.4 UTC

Gulf of Antalya 36.4N-31.75E Depth = 98 Km. Mb = 5.9

Axis	Trend	Plunge	Nodal Planes	Strike	Dip	Slip
P	161	60	plane 1	267	73	79
T	7	28	plane 2	123	20	56
B	271	11				
X	33	70				
Y	177	17				

S-wave Data:

Number of polarization angles = 13

Average error = 16.34 degrees

Standard deviation=20.09 degrees

P-wave Polarity Data:

5 inconsistencies out of 113 (4.4%)

Number of WWSSN Station Data: 25

Reference Source of data: USGS Earthquake Data Report (EDR)

Table 4

Focal Mechanism Solution for the Earthquake of 14 June 1979

Western Turkey 14 June 1979 Origin: 11:44:45.9 UTC

Aegean Sea 38.8N-26.53E Depth = 22 Km. Mb = 5.8

Axis	Trend	Plunge	Nodal Planes	Strike	Dip	Slip
P	99	69	plane 1	128	52	63
T	200	4	plane 2	268	45	59
B	291	21				
X	178	45				
Y	38	37				

S-wave Data:

Number of polarization angles = 13

Average error = 8.99 degrees

Standard deviation=11.53 degrees

P-wave Polarity Data:

2 inconsistencies out of 83 (2.4%)

Number of WWSSN Station Data: 27

Reference Source of data: USGS Earthquake Data Report (EDR)

Table 5

Focal Mechanism Solution for the Earthquake of 26 April 1981

Southwestern Turkey 26 April 1981 Origin: 14:13:27.7 UTC

Gulf of Antalya 36.6N-30.71E Depth = 70 Km. Mb = 5.4

Axis	Trend	Plunge	Nodal Planes	Strike	Dip	Slip
P	170	48	plane 1	286	80	65
T	37	31	plane 2	177	27	22
B	291	25				
X	87	63				
Y	196	9				

No S-wave Data used

P-wave Data:

2 inconsistencies out of 55 (4%)

Number of WWSSN station Data: 14

Reference Source of data: USGS Earthquake Data Report (EDR)

Figure 11 : The lower hemisphere projection of the preferred focal mechanism of the earthquake of 1 June 1977 and the graphical representation of the data. Compressional and dilatational first motions are presented as circles and triangles respectively. Solid symbols indicate that the data were read from WWSSN records. The empty symbols are for data reported in the Earthquake Data Reports. S-wave polarization angle data are plotted as short lines through a solid dot to indicate polarization patterns. The X, Y, and B axes are indicated by a circle with a solid dot. Number of inconsistent P-wave polarities and S-wave polarizations are 3 of 52 and 1 of 12 respectively.

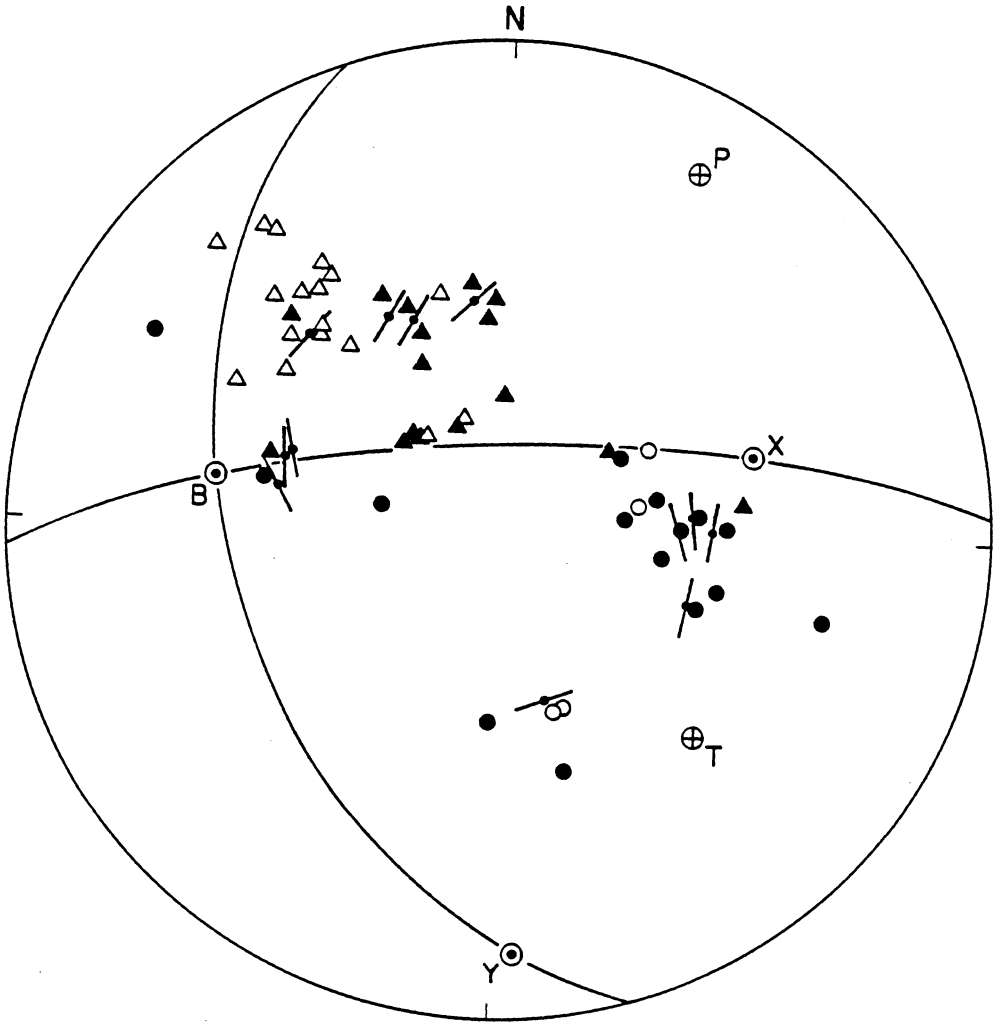
N
P
X
B
T
Y

Figure 12 : The lower hemisphere projecton of the preferred and alternative focal mechanism solutions of the earthquake of 1 June 1977. The upper and lower representations on the left show the preferred solution in terms of P, T, and B axes and in terms of fault planes. Similarly the upper and lower representations on the right show the alternative solutions. For the alternative solutions, number of inconsistencies of P and S data were raised from 3 and 1 to 5 and 3 respectively to indicate the range of solutions permitted by that decrease in data agreement.

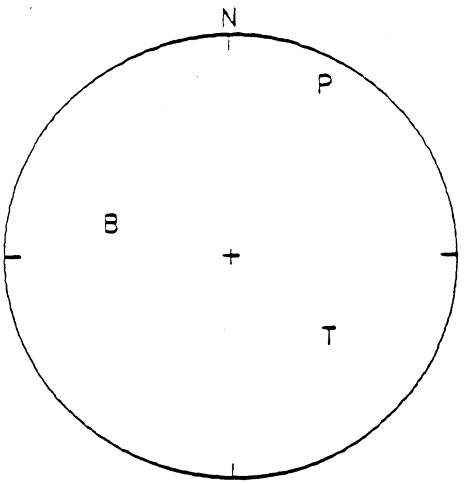
N
P
B
T

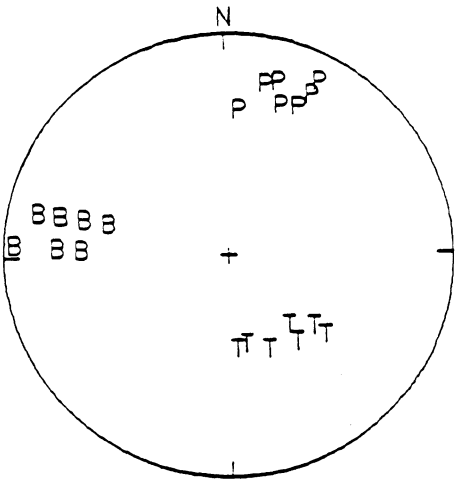
N
P
B
T

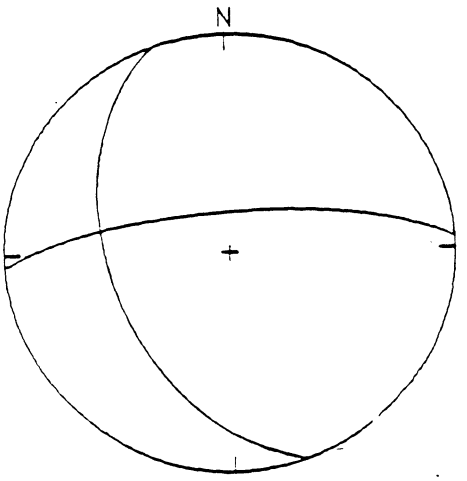
N

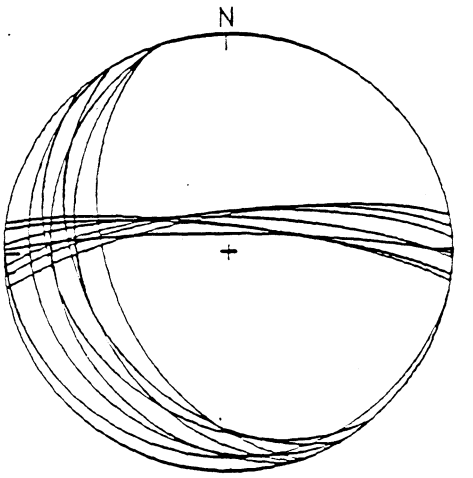
N

Figure 13 : The lower hemisphere projection of the preferred focal mechanism of the earthquake of 28 May 1979 and the graphical representation of the data. Compressional and dilatational first motions are presented as circles and triangles respectively. Solid symbols indicate that the data were read from WWSSN records. The empty symbols are for data reported in the Earthquake Data Reports. S-wave polarization angle data are plotted as short lines through a solid dot to indicate polarization patterns. The X, Y, and B axes are indicated by a circle with a solid dot. Number of inconsistent P-wave polarities and S-wave polarizations are 5 of 113 and 3 of 13 respectively.

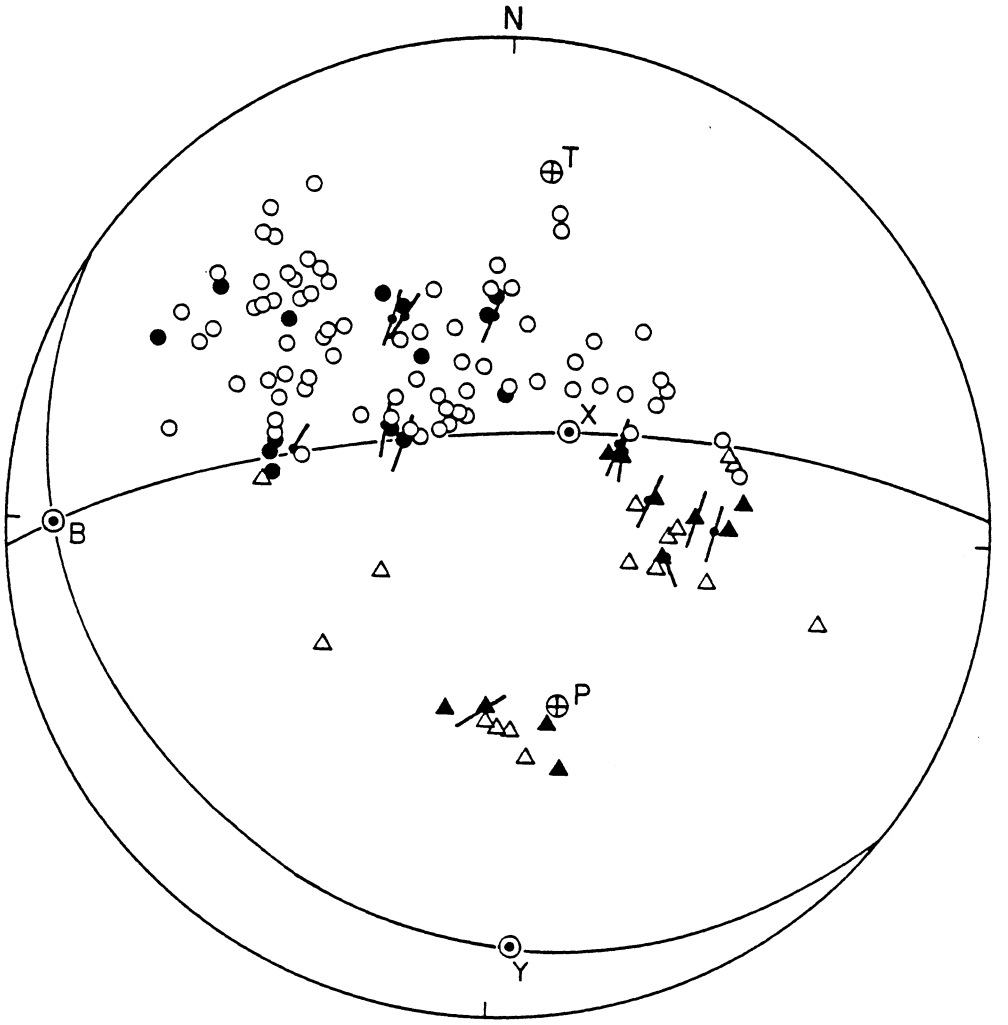
N
T
X
B
P
Y

Figure 14 : The lower hemisphere projection of the preferred and alternative focal mechanism solutions of the earthquake of 28 May 1979. The upper and lower representations on the left show the preferred solution in terms of P, T, and B axes and in terms of fault planes. Similarly the upper and lower representations on the right show the alternative solutions. For the alternative solutions, number of inconsistencies of P and S data were raised from 5 and 3 to 6 and 6 respectively to indicate the range of solutions permitted by that decrease in data agreement.

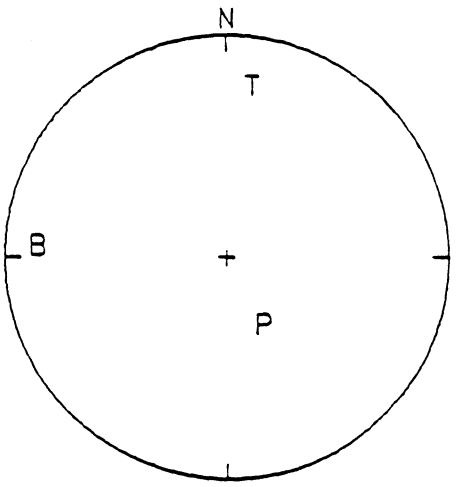
N
T
B
P

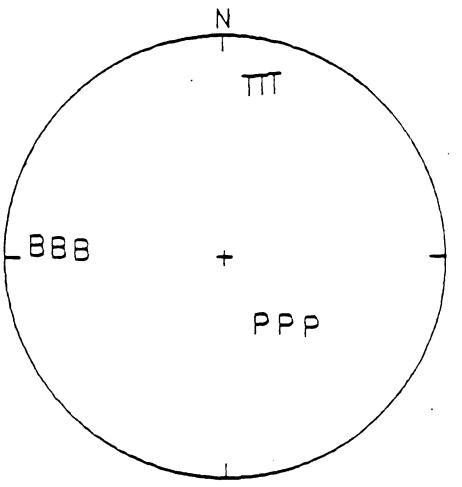
N
TTT
BBB
PPP

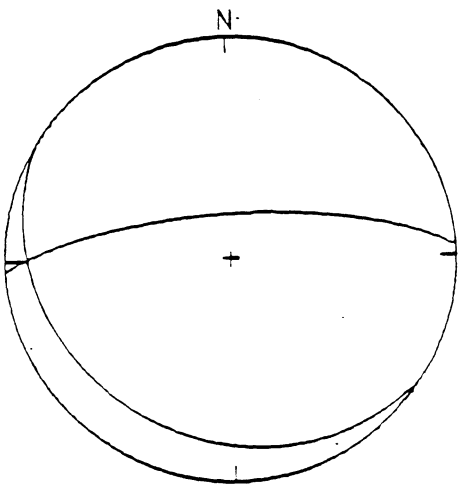
N

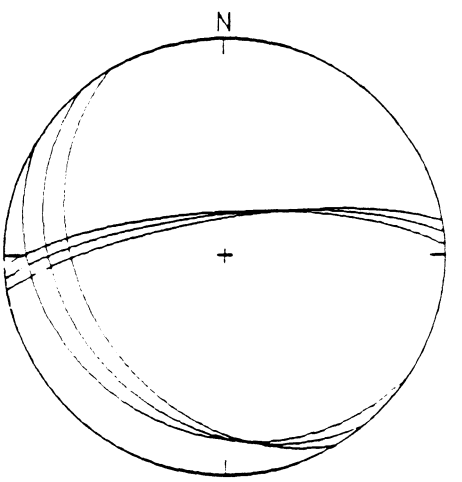
N

Figure 15 : The lower hemisphere projection of the preferred focal mechanism of the earthquake of 14 June 1979 and the graphical representation of the data. Compressional and dilatational first motions are presented as circles and triangles respectively. Solid symbols indicate that the data were read from WWSSN records. The empty symbols are for data reported in the Earthquake Data Reports. S-wave polarization angle data are plotted as short lines through a solid dot to indicate polarization patterns. The X, Y, and B axes are indicated by a circle with a solid dot. Number of inconsistent P-wave polarities and S-wave polarizations are 2 of 83 and 1 of 13 respectively.

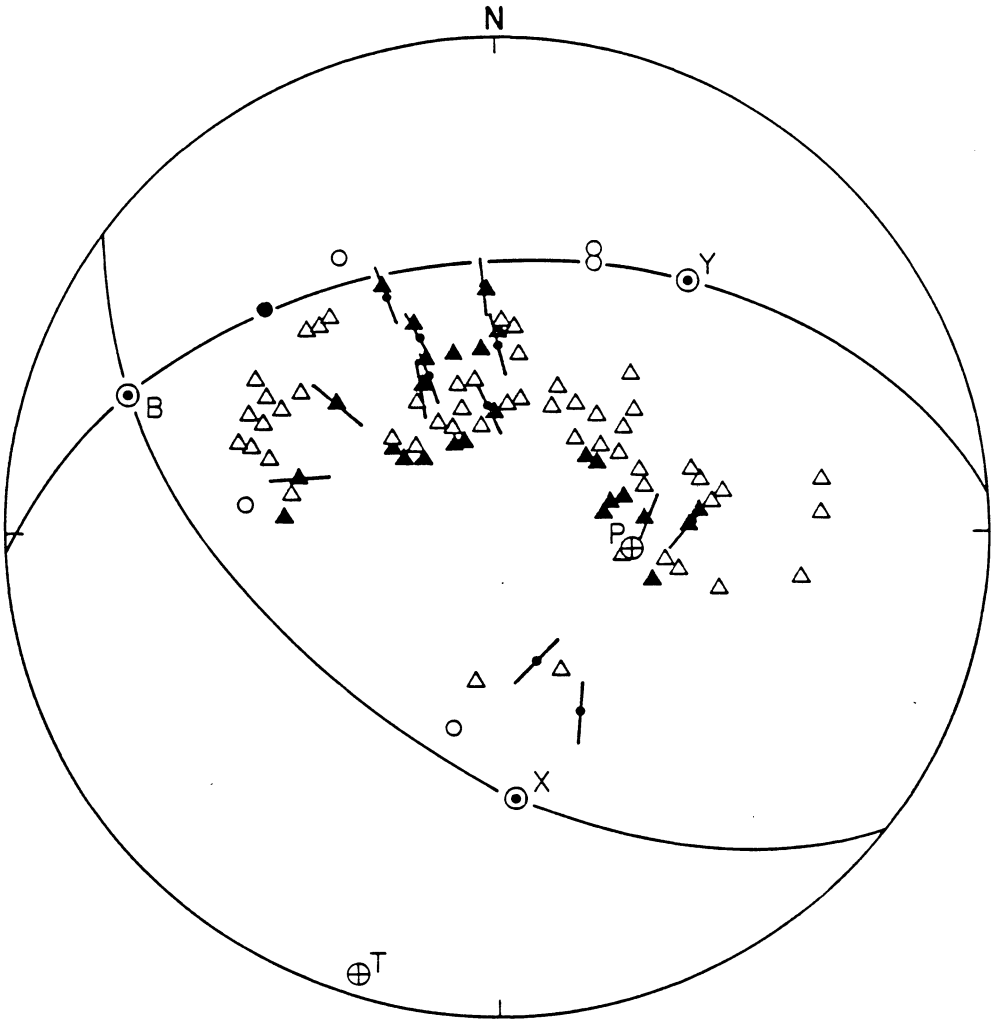
N
Y
B
P
X
T

Figure 16 : The lower hemisphere projection of the preferred and alternative focal mechanism solutions of the earthquake of 14 June 1979. The upper and lower representations on the left show the preferred solution in terms of P, T, and B axes and in terms of fault planes. Similarly the upper and lower representations on the right show the alternative solutions. For the alternative solutions, number of inconsistencies of P and S data were raised from 2 and 1 to 3 and 3 respectively to indicate the range of solutions permitted by that decrease in data agreement.

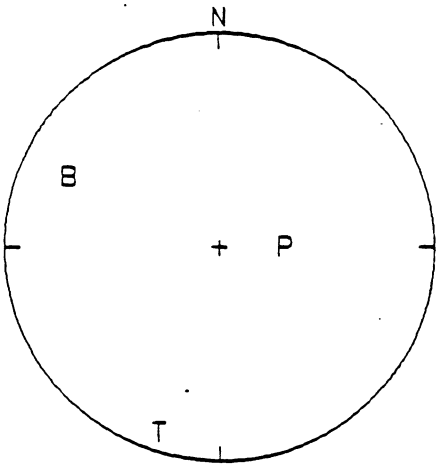
N
B
P
T

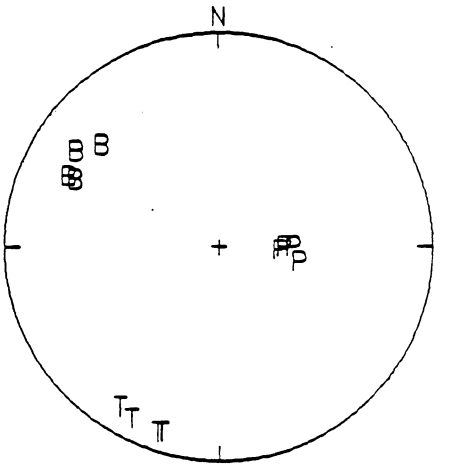
N
B
P
T

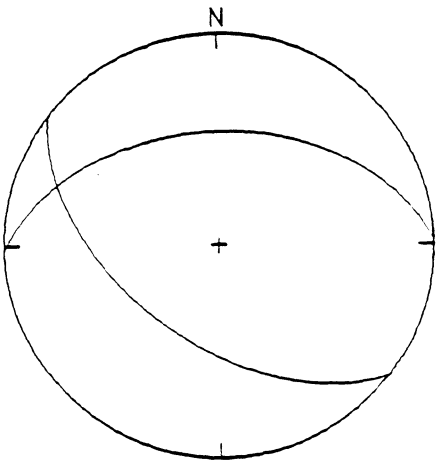
N

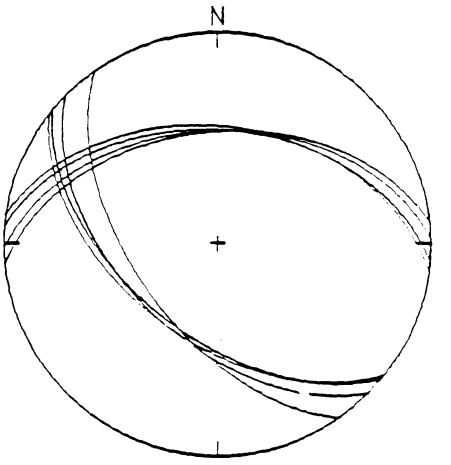
N

Figure 17 : The lower hemisphere projection of the preferred focal mechanism of the earthquake of 26 April 1981 and the graphical representation of the data. Compressional and dilatational first motions are presented as circles and triangles respectively. Solid symbols indicate that the data were read from WWSSN records. The empty symbols are for data reported in the Earthquake Data Reports. The X, Y, and B axes are indicated by a circle with a solid dot. Number of inconsistent P-wave polarities are 2 of 55. No S-wave data are used.

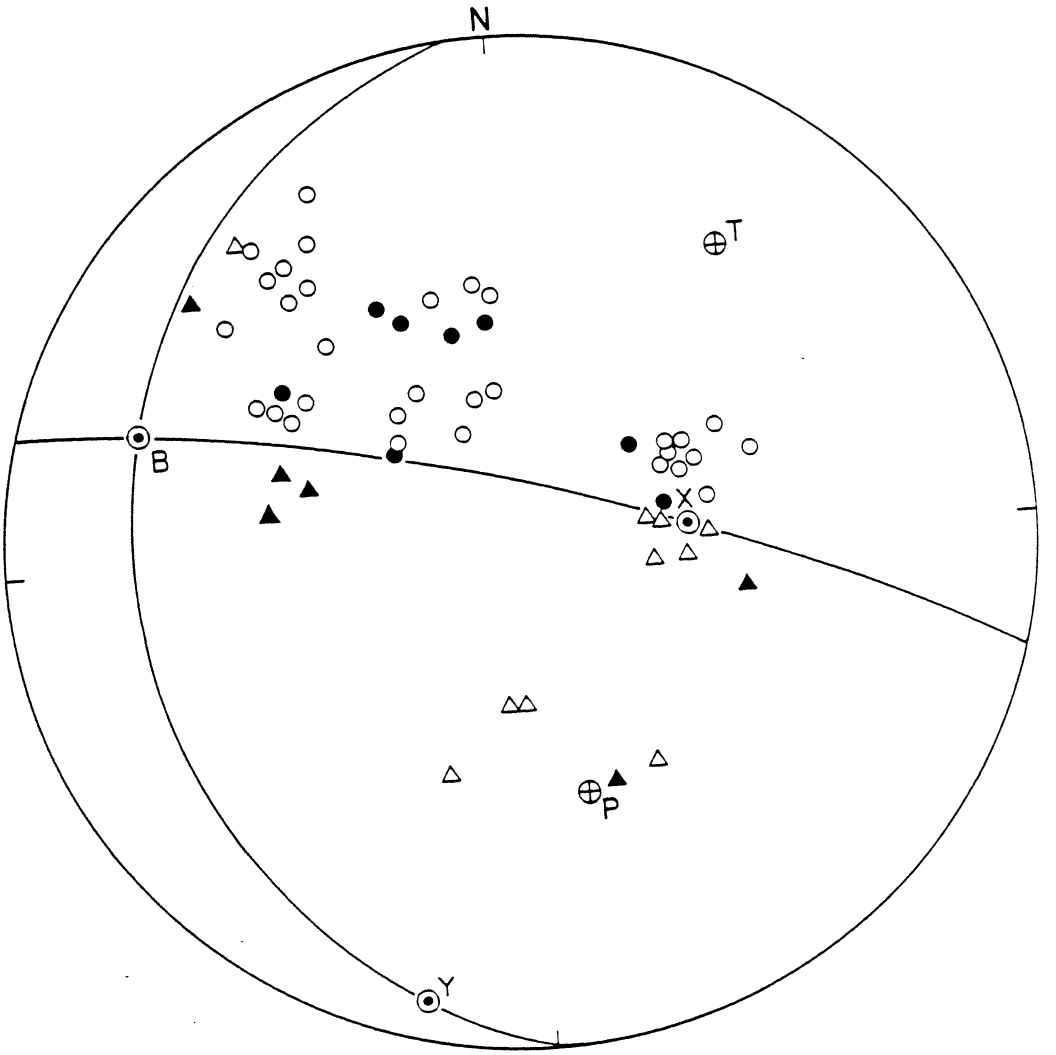
N
T
B
X
P
Y

Figure 18 : The lower hemisphere projection of the preferred and alternative focal mechanism solutions of the earthquake of 26 April 1981. The upper and lower representations on the left show the preferred solution in terms of P, T, and B axes and in terms of fault planes. Similarly the upper and lower representations on the right show the alternative solutions. For the alternative solutions, number of inconsistencies of P data were raised from 2 to 5 to indicate the range of solutions permitted by that decrease in data agreement.

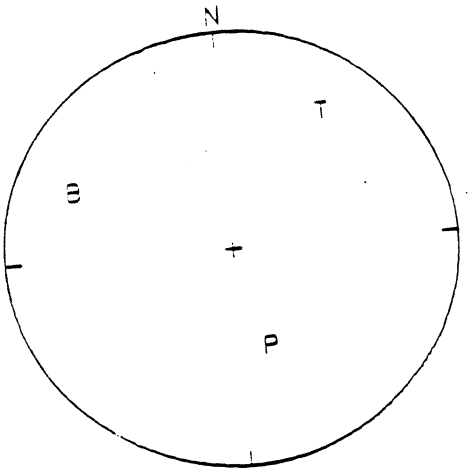
N
T
B
P

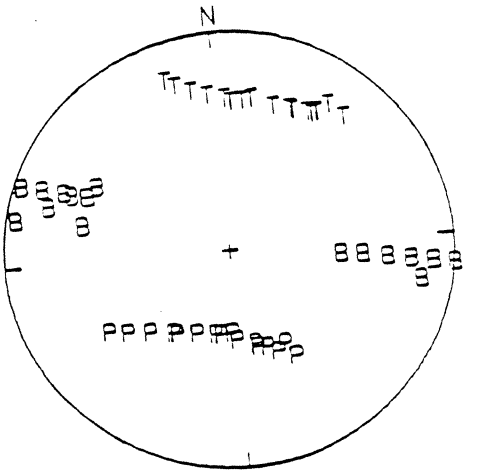
N
T
B
P

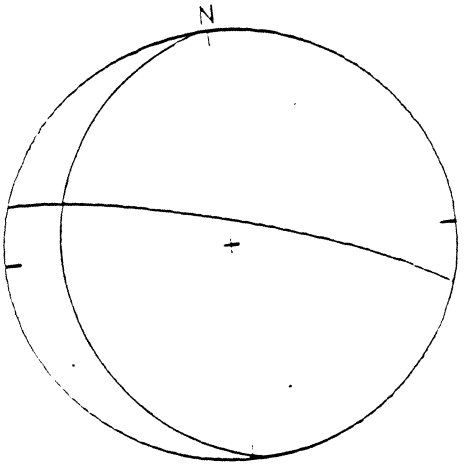
N

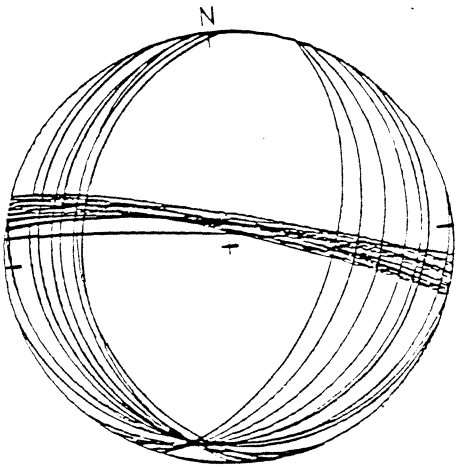
N

4. INTERPRETATION OF FOCAL MECHANISM SOLUTIONS

The focal mechanisms of three Gulf of Antalya earthquakes and one Aegean earthquake (figure 19) will be discussed in this section.

The earthquake of 1 June 1977 occurred at 36.2N latitude and 31.34E longitude in the Gulf of Antalya. The focal depth of this event was 66 kilometers, and its body wave magnitude was 5.7. A total of 52 P-wave polarities with 3 inconsistencies and 12 S-wave polarization angles with 1 P-wave inconsistency were used to develop the focal mechanism solution. Thirty-one of the 52 polarities were read from WWSSN seismograms. The average error and the standard deviation of the observed S-wave polarization angles were 10.23 and 12.01 degrees, respectively.

The focal mechanism solution indicates left-lateral strike-slip faulting (figure 11) on nodal plane one. That plane strikes 267 degrees (N87E) with a slip of 47 degrees and dips 75 degrees to the northeast. Nodal plane two, shows right- lateral motion and has a 22 degree slip, strikes 161 degrees (N19W) and dips 45 degrees to the southeast.

Nodal plane one was chosen as the probable fault plane. The following results supports that decision: (1)

the off-shore faults, inferred from the off-shore seismic profiling in the Gulf of Antalya, are parallel to the Alpine orogeny structures, namely to the Taurus Mountains which strike in the east west directions (Harsh and Kuepfer, 1980); (2) the dominant trend of the epicenters of deep or intermediate shocks is parallel to the strike direction of nodal plane one (figure 8).

The pressure axis, (P), has a considerable amount of horizontal component and its orientation is essentially in the north-south direction (NNE-SSW). The tension axis, (T), has almost equal vertical and horizontal components. The horizontal component of the tension axis is in the northeast-southwest direction. Nodal plane one indicates a combination of both strike-slip and thrust types of faulting.

Another earthquake, body wave magnitude of 5.9, occurred in the Gulf of Antalya on 28 May 1979. The focal depth was 98 kilometers and its epicenter was located at 36.4N latitude and 31.75E longitude.

One hundered thirteen P-wave polarities (5 inconsistencies) and 13 S-wave polarization angles (3 inconsistencies) were employed to obtain the focal mechanism. Twenty-five polarities were determined from WWSSN records. The average error and the standard deviation

Figure 19 : A map of the eastern Mediterranean region showing the focal mechanism solutions of the earthquakes studied at their respective locations. White = dilatational quadrants, black = compressional quadrants, arrows indicate crustal extension in western Turkey (reference (Dewey,1976) for extension).

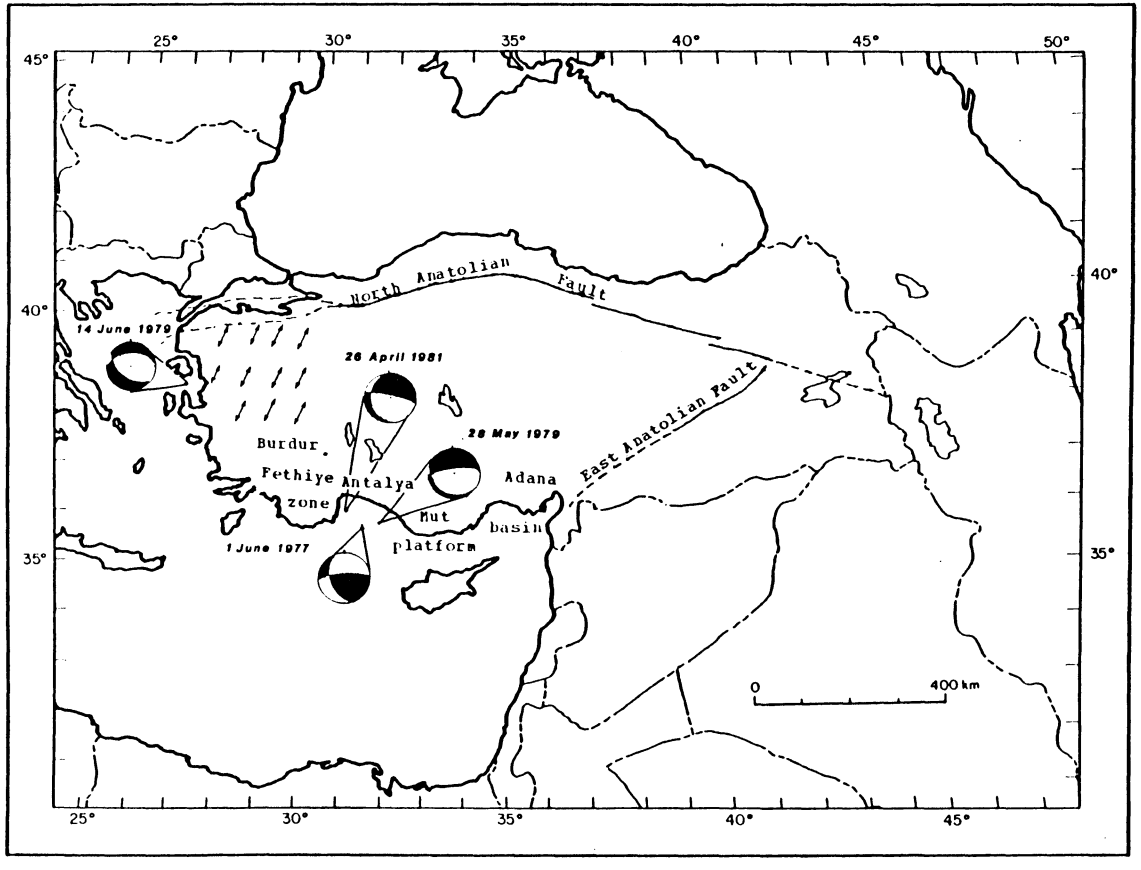
25°
30°
35°
40°
45°
50°
45°
40°
35°
North Anatolian Fault
East Anatolian Fault
14 June 1979
26 April 1981
28 May 1979
1 June 1977
Burdur
Fethiye
zone
Antalya
Mut
basin
Adana
platform
0
400 km

of S-wave polarization angles were found to be 16.34 and 20.09 degrees, respectively.

The focal mechanism solution of this event also indicates left-lateral strike-slip faulting (figure 13). Nodal plane one strikes 267 degrees (N87E) and dips 73 degrees northwest with a slip of 79 degrees. This nodal plane is almost identical to the nodal plane obtained in the focal mechanism solution for the 1 June 1977 event. The other plane, nodal plane two strikes 123 degrees (N57W) with a dip of 20 degrees to southwest with a slip of 56 degrees.

The same seismotectonic information cited in the previous focal mechanism solution, the existence of off-shore faults parallel to the Alpine structures (Harsh and Kuepfer, 1980), and alignment of epicenters of deep off-shore shocks in the east-west direction (figure 8), is consistent with this focal mechanism. Thus nodal plane one is again chosen as the fault plane. The pressure axis is primarily vertical with a small horizontal component oriented in the north-south direction (NNW-SSE) (figure 13). The tension axis is mostly horizontal and oriented in the north-south direction (NNE-SSW) as well. From the position of pressure and tension axes, and by defining nodal plane one as the fault plane, the focal mechanism solution should be strike-slip and normal faulting.

The event of 14 June 1979 occurred in the eastern Aegean Sea, just off the coast of Turkey, located at 38.8N latitude and 26.53E longitude. The body wave magnitude of the shock was 5.8, and its focal depth was 22 kilometers.

Eighty-three P-wave polarities, 27 of them from WWSSN stations, and 13 S-wave polarization angles were used for the focal mechanism solution. Two inconsistent P-wave polarities and one inconsistent S-wave polarization angle were observed in the P and S data. The average error and the standard deviation of S-wave polarization angle data were computed at 8.99 and 11.53 degrees, respectively.

The focal mechanism solution of this event is normal faulting (figure 15). Nodal plane one strikes 128 degrees (N52W) and dips 52 degrees to southwest with a slip of 63 degrees. The other plane, nodal plane two, strikes 268 degrees (N88E) and dips 45 degrees to the northwest with a 59 degrees slip. The pressure axis, which is nearly vertical, has a small horizontal component with an orientation in the east-west direction. Unlike the pressure axis, the tension axis is almost horizontal and oriented in the northeast and southwest directions.

There is no reason to prefer either plane as the fault plane due to the scattered distribution of seismicity in this region (figure 2). Nevertheless, plane two is

hypothesized to be the fault plane because its strike direction is parallel to the east-west oriented grabens in western Turkey. Additionally, the focal mechanism solutions in the eastern Aegean (McKenzie, 1972 and Alptekin, 1973) indicate east-west striking normal faulting. The geology of the graben systems in western Turkey also indicates the continuation of these grabens in the eastern Aegean (Arpat and Bingol, 1969 in Dewey and Sengor, 1979).

The third Gulf of Antalya earthquake whose focal mechanism was obtained in this study, occurred at 36.6N latitude and 30.71E longitude on 26 April 1981. The focal depth and body wave magnitude of this event were 70 kilometers and 5.4, respectively.

For the focal mechanism determination, 55 P-wave first motions, including 2 inconsistencies, employed only. Fourteen of the first motions were read from WWSSN records. The solution of the focal mechanism shows left-lateral strike-slip faulting (figure 17). Nodal plane one strikes 286 degrees (N74W) and dips 80 degrees to the northeast, whereas nodal plane two strikes 177 degrees (N3W) with a 27 degree dip to the southwest. Both nodal planes, one and two, have slips of 65 and 22 degrees, respectively.

The pressure axis has both vertical and horizontal components. The horizontal component of the pressure axis

is oriented in the north-south direction (NNW-SSE). The horizontal component of the tension axis is oriented in the northeast and southwest directions.

The existence of off-shore faults parallel to the Alpine structures (Harsh and Kuepfer, 1980), and the alignment of epicenters in the northern Gulf of Antalya and inland suggest that nodal plane one is the fault plane (figures 7 and 8). The choice of nodal plane one as the fault plane indicates that this event is a combination of strike-slip and normal faulting.

5. DISCUSSION AND CONCLUSIONS

The computer derived focal mechanism solutions (based on P-wave polarities and S-wave polarization angles) for three earthquakes in the Gulf of Antalya area indicated combined strike-slip normal faulting for the 28 May 1979 and 26 April 1981 events, and combined strike-slip thrust faulting for the 1 June 1977 event. The epicenters for these events occurred within 50 kilometers or less from each other, and their focal depths ranged from 66 to 98 kilometers. All of the nodal planes chosen as the fault planes strike in an east-west direction and dip northward at 73 to 80 degrees.

The occurrence of the opposite type of faulting at almost same depths (66 and 70 kilometers) and with a small horizontal seperation indicates a change of stress direction. Thus, the focal mechanism solutions of the Gulf of Antalya earthquakes determined in this study support the interpretation of complex tectonics in the region.

The seismic activity studied is due to stress concentrations resulting in the Fethiye zone, southwestern Turkey (Erdik and others, 1982). Also, various types of faults inferred from the previous focal mechanism solutions there (McKenzie, 1972 and Alptekin and Ezen, 1978) also

indicate the complexity of the tectonics in the region. Obviously, many additional focal mechanism solutions are needed to understand the present tectonics of the eastern Mediterranean Sea.

The focal mechanism solution of the Aegean earthquake of 14 June 1979 is in agreement with the previous focal mechanism solutions obtained by McKenzie (1972) and Alptekin (1973). Its solution indicates that the east-west oriented graben systems associated with the normal faults in western Turkey are extended into the eastern Aegean.

The tension axis of the solution of the Aegean earthquake is almost horizontal and aligned in the northeast and southwest directions. The pressure axis is almost vertical with only a small horizontal component. Thus, the solution is consistent with the theory of the crustal extension in western Turkey (Dewey and Sengor, 1979 and Alptekin, 1973) resulting from the rapid westward movement of the Turkish plate.

REFERENCES

Allen, C. R., 1969, Active faulting in northern Turkey, Division of Geological Sciences, Contribution No.1577, California Institute of Technology, Pasadena, California.

Alptekin, O., 1973, Focal mechanisms of earthquakes in western Turkey and their tectonic implications, Ph.D. thesis, New Mexico Institute of Mining and Technology, Socorro.

Alptekin, O., and Ezen, U., 1978, Focal mechanisms of some earthquakes in the region surrounding the Akkuyu nuclear power plant site, Technical University of Istanbul report.

Ambraseys, N. N., 1970, Some characteristic features of the North Anatolian Fault Zone, Tectonophysics, vol. 9, pp. 143-165.

Arpat, E., and Bingol, E., 1969, Some thoughts about graben systems in the Aegean region, Bull. Mineral Res. Exploration Ins. Turkey, no. 73 pp. 1-9, (in Turkish).

Canitez, N., and Toksoz, M. N., 1971, Focal mechanism and source depth of earthquakes from body and surface wave data, Bull. Seism. Soc. Am., vol. 61, no. 5, pp. 1369-1379.

Dewey, J. W., 1976, Seismicity of Northern Anatolia, Bull. Seism. Soc. Am. vol. 66, no. 3, pp. 843-868.

Dewey, J. W., and Sengor, A. M. C., 1979, Aegean and surrounding regions: Complex multiplate and continuum tectonics in a convergent zone, Geol. Soc. Am. Bull. part 1. vol. 90, pp. 84-92.

Erdik, M., Doyuran, V., Yucemen, S., Gulhan, P., and Akkas, N., 1982, A probabilistic assesment of the seismic hazard in Turkey for long return periods, proceedings, Third International Micronization Conference, June 28-July 1, 1982, Seattle, WA. pp. 1261-1272.

Ergin, K., Guclu, U., and Uz, Z., 1967, A catalog of earthquakes for Turkey and surrounding area, Technical University of Istanbul press.

Ergin, K., and Buyukasikoglu, S., 1978, Seismicity of Akkuyu nuclear power plant-site, final report, Technical University of Istanbul report, 162 pages.

Gilluly, I., 1972, Tectonics involved in the evaluation of mountain ranges, in the Nature of the Solid Earth, edited by E. C. Robertson, McGraw-Hill, New York, pp. 406-439.

Guinn, S., 1977, Earthquake focal mechanisms in the southeastern United States, Nuclear Regulatory Commission publication NUREG/CR-1503, Washington D.C., June 1980, pp. 1-150.

Harsch, W., and Kuepfer, T., 1980, Seismotectonic implications of relative motions between the African, Arabian, and Turkish plates. In Proc. of 7th World Conf. on Earthq. Eng., vol. 1, held Sept 1980. pp. 253-260.

Hermann, R. B., 1975, A student guide to the use of P and S wave data for focal mechanism determination, Earthquake Notes, vol. 46, no. 4, pp. 29-39.

Ilhan, E., 1971, The structural features of Turkey, in Geology and History of Turkey edited by A. S. Cambell, The Petrol. Explor. Soc., Tripoli, Libya, pp. 159-170.

Ketin, I., 1968, Relations between general tectonic features and the main earthquake regions of Turkey, Bull. Min. Res. and Explor. Inst. (M.T.A.), no. 71, pp. 63-67, Ankara, Turkey.

Ketin, I., 1969, Ueber die Nordanatolische horizontal verschiebung. Bull. Min. Res. and Explor. Inst., Turkey, Foreign ed. no. 72 pp. 1-28.

McKenzie, D., 1972, Active tectonics of the Mediterranean Region, Geophys. J. R. Astr. Soc., vol. 30, pp. 109-185.

Nuttli, O., 1964, The determination of S-wave polarization angles for an earth model with crustal layering. Bull. Seism. Soc. Am., vol. 54, no. 5, part A, pp. 1429-1440.

Papazachos, B. C., 1976, Seismotectonics of the northern Aegean area, Tectonophysics, vol. 46, pp. 285-296.

Pavioni, N., 1961, Die Nordanatolische Horizontal verschiebung. Geol. Rundschau, 51.

Ryan, B. F., Stanley, D. J., Hersey, J. B., Fahlquist, D. A., and Allan, T.D., 1970, The tectonics and geology of the Mediterranean Sea, in the Sea edited by A. E. Maxwell, Wiley-interscience, vol. 4, pp. 382-492.

Stauder, W. S. J., and Bollinger, G. A., 1964, The S-wave project for focal mechanism studies earthquakes of 1962, 1963, 1964. A scientific report. Department of Geophysics and Geophysical Engineering, Institute of Technology, Saint Louis University, 308 pages.

Toksoz, M. N., Shakal, A. F., and Michael, A. J., 1979, Space-time migration of earthquakes along the North Anatolian Fault zone and seismic gaps, Pure and Applied Geophysics, no. 117, pp. 1258-1270.

APPENDIX: DATA TABULATIONS

Data Tabulation for Event Number 1:

Southwestern Turkey
Gulf of Antalya

1 June 1977
36.2N-31.34E

Origin: 12:54:49.2 UTC
Depth = 66 Km. Mb = 5.7

			P wave Data			S wave Data	
STA	D(deg)	AZ(deg)	Phase	ih(deg)	jh(deg)	E(deg)#	Quality$
ZAG	15.01	314	IPD*	70	-	-	-
AQU	15.16	299	IPC	70	-	-	-
SOP	15.83	321	IPD*	68	-	-	-
VKA	16.34	322	EPD*	66	-	-	-
PRU	18.36	324	IPD*	58	-	-	-
SHI	18.94	104	IPC	57	-	-	-
FUR	18.99	315	IPD*	56	-	-	-
BRG	19.24	325	IPD*	56	-	-	-
GRF	19.86	319	EPD*	53	-	-	-
MOX	20.22	322	IPD*	52	-	-	-
SPF	20.23	299	IPD*	52	-	-	-
STU	20.49	315	EPD	52	48	85	fair
WLS	21.40	312	IPD*	49	-	-	-
HOK	22.66	318	IPD*	46	-	-	-
LBF	22.99	306	IPD*	46	-	-	-
LOR	23.16	307	IPD*	45	-	-	-
COP	23.33	332	IPD	45	41	56	good
NUR	24.66	352	IPD	43	40	54	good
UPP	25.24	344	IPD*	42	-	-	-
KON	27.33	336	IPD	41	39	52	good
AAE	27.92	164	EPC	41	39	85	good
TOL	27.99	288	EPD	41	39	69	good
MAL	28.65	282	EPC	41	38	45	good
ESK	30.28	320	IPD*	40	-	-	-
KBL	30.66	82	IPD	40	-	-	-
PTO	31.36	291	-	-	38	56	good
KEV	33.65	357	EPD	40	-	-	-
NDI	39.14	88	IPC	38	36	-77	good
POO	41.29	104	IPC	37	-	-	-
KBS	43.53	355	IPD	36	-	-	-
KTG	44.20	337	EPD	36	-	-	-
KOD	49.05	110	IPC	34	34	83	good
SHL	52.28	84	IPC	33	33	90	good
GDH	54.85	334	EPD	32	-	-	-
BUL	56.14	183	EPC	31	-	-	-

			P wave Data		S wave Data		
STA	D(deg)	AZ(deg)	Phase	ih(deg)	jh(deg)	E(deg)#	quality$
FRR	56.78	162	IPC*	31	-	-	-
AVY	57.01	161	IPC*	31	-	-	-
CHG	61.32	87	IPC	30	30	78	good
PEK	64.34	58	IPC*	29	-	-	-
SNG	69.09	97	IPC	27	-	-	-
HKC	71.60	76	EPC	26	-	-	-
SHK	78.41	56	EPC	24	-	-	-
COL	79.19	360	EPD	24	-	-	-
BAG	79.89	77	EPC*	23	-	-	-
MAT	80.79	51	EPD	23	-	-	-
AAM	81.88	317	EPD	22	-	-	-
BLA	83.39	312	EPD	22	-	-	-
FVM	88.60	318	EPD	20	-	-	-
DAV	89.26	82	EPC	20	-	-	-
CAR	90.44	283	EPC	20	-	-	-
NEW	91.29	340	IPD*	20	-	-	-
MSO	91.62	337	EPD	20	-	-	-
TUL	93.01	320	IPD*	20	-	-	-

* : Phase determined from Earthquake Data Report (EDR)
# : E(deg) = Observed S-wave polarization angle in degrees
$: Quality = Difference (Delta) between observed S-wave polarization angle and the theoretical S-wave polarization angle specified by the focal mechanism solution obtained.
Delta less than 20 degrees = Good
Delta between 20 and 25 degrees = Fair
Delta grater than 25 degrees = Poor

Data Tabulation for Event Number 2:

Southwestern Turkey
Gulf of Antalya

28 May 1979 Origin: 09:27:32.4 UTC
36.4N-31.75E Depth = 98 Km. Mb = 5.9

			P wave Data		S wave Data		
STA	D(deg)	AZ(deg)	Phase	ih(deg)	jh(deg)	E(deg)#	Quality$
SRO	15.12	323	IPC*	69	-	-	-
SPC	15.29	330	IPC*	69	-	-	-
AQU	15.37	298	IPC	68	-	-	-
ANS	15.77	303	EPC*	67	-	-	-
SOP	15.91	320	IPC*	66	-	-	-
CEY	16.02	311	IPC*	66	-	-	-
TRI	16.41	310	IPC	65	-	-	-
VKA	16.41	321	EPC*	65	-	-	-
FIR	17.30	301	IPC*	61	-	-	-
BOL	17.48	304	EPC*	61	-	-	-
BHG	17.95	315	IPC*	59	-	-	-
CGL	17.96	286	IPC*	59	-	-	-
KHC	18.37	319	IPC*	58	-	-	-
PRU	18.42	323	IPC*	58	-	-	-
OGA	18.63	311	IPC*	57	-	-	-
SHI	18.66	105	IPD*	57	-	-	-
WET	18.75	319	IPC*	56	-	-	-
GAP	18.89	312	IPC*	56	-	-	-
OBN	19.00	9	IPC*	56	-	-	-
FUR	19.10	314	IPC*	55	-	-	-
BRG	19.29	324	IPC*	55	-	-	-
MOS	19.74	10	IPC*	53	-	-	-
GRF	19.95	318	IPC*	53	-	-	-
HOF	19.96	320	IPC*	53	-	-	-
CLL	20.03	324	IPC*	52	-	-	-
SPF	20.44	298	IPC*	51	-	-	-
STU	20.61	314	IPC	51	-	-	-
BAF	21.52	310	IPC*	49	-	-	-
SSB	22.33	302	IPC*	47	-	-	-
BUG	23.02	318	IPC*	45	-	-	-
SMF	23.15	305	IPC*	45	-	-	-
COP	23.24	332	IPC	45	41	46	good
PUL	23.40	358	IPC*	45	-	-	-
HEE	23.44	316	IPC*	45	-	-	-
CAF	23.97	300	IPC*	44	-	-	-
WIT	24.06	321	IPC*	44	-	-	-

			P wave Data		S wave Data	
STA	D(deg)	AZ(deg)	Phase	ih(deg)	jh(deg)	E(deg)#	Quality$
EPF	24.95	295	IPC*	43	-	-	-
UPP	25.18	343	IPC*	43	-	-	-
SSC	26.25	308	IPC*	42	-	-	-
SGR	26.57	305	IPC*	42	-	-	-
ARU	26.96	34	IPC*	42	-	-	-
LGR	27.01	293	IPC*	42	-	-	-
KON	27.31	335	IPC	41	39	54	good
ALM	27.38	281	IPD*	41	-	-	-
SAM	27.84	72	EPD*	41	-	-	-
KJF	27.93	356	IPC*	41	-	-	-
AAE	27.99	165	IPD	41	-	-	-
TOL	28.25	288	IPC	41	-	-	-
MAL	28.94	282	IPC	41	-	-	-
DSH	29.33	75	IPC*	41	-	-	-
KBL	30.31	82	IPD	41	-	-	-
APA	31.20	1	IPC*	41	-	-	-
DKM	31.32	315	IPC*	41	-	-	-
PTO	31.61	291	IPC	41	38	-81	poor
ANR	31.84	70	EPD*	41	-	-	-
FRU	33.36	66	IPC*	40	-	-	-
KEV	33.51	357	IPC	40	38	21	good
NAI	37.78	172	IPD*	38	-	-	-
NDI	38.80	88	EPD	38	37	-70	good
NVS	39.45	45	IPC*	38	-	-	-
ELT	41.08	48	IPC*	37	-	-	-
AKU	41.13	331	IPC*	37	-	-	-
KBS	43.40	355	EPC	36	-	-	-
KTG	44.17	337	IPC*	36	-	-	-
NRI	44.69	25	IPC*	36	-	-	-
KIC	44.79	237	IPD*	36	-	-	-
PDA	45.20	290	IPC	36	-	-	-
HYB	45.33	102	IPD*	36	-	-	-
KHE	45.44	6	IPC*	36	-	-	-
DAG	46.12	346	IPC*	35	-	-	-
MOY	50.17	49	IPC*	34	-	-	-
SHL	51.94	84	IPD	33	34	-65	good
CLK	51.89	176	IPD*	33	-	-	-
MTD	52.90	180	IPD*	33	-	-	-
GDH	54.85	334	IPC	32	-	-	-
BOD	56.21	40	IPC*	32	-	-	-
BUL	56.32	184	IPD*	32	-	-	-
AVY	57.06	162	IPD*	31	-	-	-
TIK	58.08	22	IPC*	31	-	-	-
WIN	60.27	196	IPD	30	-	-	-
STJ	60.83	309	EPC*	30	-	-	-

			P wave Data		S wave Data	
STA	D(deg)	AZ(deg)	Phase	ih(deg)	jh(deg)	E(deg)#	Quality$
CHG	60.98	87	IPD*	30	-	-	-
YAK	62.07	32	IPC*	30	-	-	-
FRB	62.28	330	IPC*	30	-	-	-
PRE	61.92	184	IPD	30	30	51	good
RES	63.79	346	IPC*	29	-	-	-
PCT	65.15	90	IPD*	29	-	-	-
SCH	65.63	321	EPC*	29	-	-	-
MBC	66.13	353	IPC*	28	-	-	-
CN2	68.29	51	EPC*	28	-	-	-
SNG	68.78	97	EPD	28	28	61	poor
TSI	69.33	101	EPD*	27	-	-	-
SEY	70.31	25	IPC*	27	-	-	-
HKC	71.24	76	EPD	27	-	-	-
ILT	73.51	12	IPC*	26	-	-	-
MNT	74.35	315	EPC*	25	-	-	-
WES	74.83	312	EPC	25	26	56	good
FCC	75.04	334	IPC*	25	-	-	-
IMA	77.76	2	IPC*	24	-	-	-
YKC	77.77	345	IPC*	24	-	-	-
SHK	78.04	56	EPD	24	25	-49	good
COL	79.02	360	iPC*	23	-	-	-
BAG	79.53	77	IPD	24	25	-54	good
MAT	80.43	52	EPD	23	24	-34	good
FFC	80.92	335	IPC*	23	-	-	-
AAM	81.98	317	IPC*	23	-	-	-
BLA	83.52	312	EPC	22	23	64	fair
EDM	85.74	340	IPC*	21	-	-	-
TRT	87.25	102	IPD*	21	-	-	-
FVM	88.70	318	IPC*	21	-	-	-
BAO	91.14	251	EPD*	20	-	-	-
BDW	93.66	333	IPC*	20	-	-	-
LON	93.88	342	IPC*	20	-	-	-
GOL	94.60	328	IPC*	20	-	-	-

* : Phase determined from Earthquake Data Report (EDR)
\# : E(deg) = Observed S-wave polarization angle in degrees
$: Quality = Difference (Delta) between observed S-wave polarization angle and the theoretical S-wave polarization angle specified by the focal mechanism solution obtained.
Delta less than 20 degrees = Good
Delta between 20 and 25 degrees = Fair
Delta grater than 25 degrees = Poor

Data Tabulation for Event Number 3:

Western Turkey Aegean Sea — 14 June 1979 38.8N-26.53E — Origin: 11:44:45.9 UTC Depth = 22 Km. Mb = 5.8

			P wave Data		S wave Data		
STA	D(deg)	AZ(deg)	Phase	ih(deg)	jh(deg)	E(deg)#	Quality$
GRS	15.39	81	IPD*	56	-	-	-
TAB	15.54	87	IPD*	56	-	-	-
STU	15.96	314	EPC	55	-	-	-
BRN	16.46	330	EPC*	54	-	-	-
KER	17.11	99	EPD*	52	-	-	-
OBN	17.66	19	IPC*	51	-	-	-
SMF	18.37	303	IPD*	49	-	-	-
MOS	18.49	20	IPC*	49	-	-	-
HEE	18.85	317	EPD*	48	-	-	-
WTS	19.04	320	EPD*	48	-	-	-
CAF	19.18	296	IPD*	47	-	-	-
COP	19.34	335	EPD	47	45	4	good
TCF	19.36	301	IPD*	47	-	-	-
LFF	20.11	296	IPD*	45	-	-	-
EPF	20.20	290	IPD*	45	-	-	-
MFF	21.02	300	IPD*	43	-	-	-
ALI	21.10	277	IPC*	42	-	-	-
SSC	21.50	306	IPD*	42	-	-	-
NUR	21.76	357	EPD	41	41	-22	poor
LPF	21.95	304	IPD*	41	-	-	-
LGR	22.28	289	IPD*	40	-	-	-
KAT	23.07	80	IPD*	39	-	-	-
SHI	23.30	105	IPD*	38	-	-	-
KON	23.47	338	EPD	38	37	-4	good
MAL	24.49	275	IPD	37	-	-	-
ASH	24.90	82	IPD*	36	-	-	-
KJF	25.44	1	IPD*	36	-	-	-
MTE	26.20	284	EPD*	35	-	-	-
PTO	26.91	286	IPD	35	35	-19	good
ARU	27.52	40	IPD*	35	-	-	-
VAL	28.64	309	EPD	35	34	2	good
APA	29.04	5	IPD*	35	-	-	-
KEV	31.01	0	EPD	34	34	-14	good
SAM	31.17	75	IPD*	34	-	-	-
AAE	31.62	156	-	-	34	31	good
TAS	32.59	72	IPD*	34	-	-	-

			P wave Data			S wave Data	
STA	D(deg)	AZ(deg)	Phase	ih(deg)	jh(deg)	E(deg)#	Quality$
KBL	34.14	84	IPD	34	-	-	-
BNG	34.98	194	IPC*	33	-	-	-
KTG	40.35	337	EPD	32	32	4	good
KBS	40.66	356	EPD	32	-	-	-
NVS	40.82	48	IPD*	32	-	-	-
NAI	40.99	164	-	-	32	61	good
ELT	42.65	50	IPD*	31	-	-	-
DAG	42.78	346	IPD	31	-	-	-
NDI	42.87	88	IPD	31	32	-46	good
KHE	43.53	7	IPD*	31	-	-	-
POO	45.60	102	IPD	30	-	-	-
HYB	49.86	100	IPD*	29	-	-	-
GDH	50.86	333	EPD	29	29	16	good
MOY	51.77	50	IPD*	28	-	-	-
KOD	53.50	108	IPD	28	-	-	-
BOD	57.01	40	IPD*	27	-	-	-
TIK	57.38	22	IPD*	27	-	-	-
FRB	58.11	329	EPD*	26	-	-	-
LZH	59.67	66	IPD*	26	-	-	-
RES	60.43	345	EPD*	26	-	-	-
WIN	61.69	190	IPD*	25	-	-	-
YAK	62.21	31	IPD*	25	-	-	-
CDU	62.45	72	IPD*	25	-	-	-
MBC	63.18	351	EPD*	25	-	-	-
CHG	64.98	85	IPD	25	25	-61	good
BJI	66.20	57	IPD*	24	-	-	-
MNT	69.70	312	IPD*	23	-	-	-
SEY	69.81	23	IPD*	23	-	-	-
CN2	69.96	50	IPD*	23	-	-	-
WES	70.11	309	EPD	23	-	-	-
ILT	71.92	10	IPD*	22	-	-	-
TSI	73.83	99	EPD*	22	-	-	-
YKC	74.30	342	EPD*	22	-	-	-
HKC	74.62	74	IPD	22	-	-	-
IMA	75.46	0	EPD*	21	-	-	-
COL	76.53	358	IPD	21	21	-23	good
ANM	76.54	5	EPD*	21	-	-	-
FFC	76.93	332	IPD*	21	-	-	-
YSS	77.34	39	IPD*	21	-	-	-
AN7	78.47	313	EPD*	21	-	-	-
BLA	78.81	309	EPD	20	-	-	-
SHK	80.05	54	IPD	20	-	-	-
EDM	81.98	337	IPD*	19	-	-	-
MAT	82.09	49	IPD	19	-	-	-
BAG	82.98	75	IPD	19	-	-	-

			P wave Data		S wave Data		
STA	D(deg)	AZ(deg)	Phase	ih(deg)	jh(deg)	E(deg)#	Quality$
SIT	83.28	350	EPD*	19	-	-	-
FVM	84.11	315	IPD	19	-	-	-
MSO	87.71	334	EPD	18	-	-	-
LON	90.24	339	IPD	17	-	-	-
DAV	92.60	79	EPD	17	-	-	-

* : Phase determined from Earthquake Data Report (EDR)
\# : E(deg) = Observed S-wave polarization angle in degrees
$: Quality = Difference (Delta) between observed S-wave polarization angle and the theoretical S-wave polarization angle specified by the focal mechanism solution obtained.
Delta less than 20 degrees = Good
Delta between 20 and 25 degrees = Fair
Delta grater than 25 degrees = Poor

Data Tabulation for Event Number 4:

Southwestern Turkey 26 April 1981 Origin: 14:13:27.7 UTC
Gulf of Antalya 36.6N-30.71E Depth = 70 Km. Mb = 5.4

			P wave Data		S wave Data		
STA	D(deg)	AZ(deg)	Phase	ih(deg)	jh(deg)	E(deg)#	Quality$
SOP	15.26	321	EPD*	69	-	-	-
KRA	15.58	333	IPC*	68	-	-	-
TRI	15.68	311	EPD	68	-	-	-
VKA	15.77	322	EPC*	68	-	-	-
KSP	17.63	329	EPC*	61	-	-	-
KHC	17.72	321	IPC*	61	-	-	-
PRU	17.80	324	IPC*	60	-	-	-
OGA	17.90	311	IPC*	60	-	-	-
HOF	19.32	321	IPC*	55	-	-	-
CLL	19.42	325	IPC*	55	-	-	-
SSB	21.54	302	IPC*	49	-	-	-
LOR	22.56	307	IPC	46	-	-	-
COP	22.81	333	IPC	46	-	-	-
WTS	22.89	320	EPC*	46	-	-	-
MZF	23.10	303	IPC*	45	-	-	-
NUR	24.28	353	IPC*	43	-	-	-
UPP	24.80	344	IPC*	43	-	-	-
MFF	25.03	303	IPC*	42	-	-	-
SSC	25.50	308	IPC*	42	-	-	-
KON	26.83	336	IPC	41	-	-	-
TDD	26.99	153	IPD*	41	-	-	-
KJF	27.73	357	IPC*	41	-	-	-
MAL	28.09	281	EPD	41	-	-	-
AAE	28.37	163	EPD	41	-	-	-
PTO	30.78	291	EPD	40	-	-	-
BNG	33.87	202	IPD*	40	-	-	-
KSH	35.50	71	IPC*	39	-	-	-
POO	41.86	104	IPD	37	-	-	-
KBS	43.17	355	IPC	36	-	-	-
WMQ	43.38	62	IPC*	36	-	-	-
PDA	44.36	289	IPD	36	-	-	-
DAG	45.77	346	IPC	35	-	-	-
ALE	54.40	351	EPC*	32	-	-	-
LZH	57.52	67	IPC*	31	-	-	-
BTO	60.12	60	IPC*	30	-	-	-
KMI	61.60	79	IPC*	30	-	-	-

			P wave Data		S wave Data	
STA	D(deg)	AZ(deg)	Phase	ih(deg)	jh(deg)	E(deg)#	Quality$
FRB	61.73	330	IPC*	30	-	-	-
PRE	62.02	183	IPD*	30	-	-	-
BDT	62.70	88	IPD*	29	-	-	-
BJI	64.60	58	IPC*	29	-	-	-
SCH	64.99	321	EPC*	29	-	-	-
BLF	65.46	184	IPD*	28	-	-	-
TIA	67.07	61	IPC*	28	-	-	-
WHN	67.86	68	IPC*	28	-	-	-
IPM	71.52	98	EPD*	26	-	-	-
SSE	72.60	64	IPC*	26	-	-	-
MNT	73.66	315	IPC*	25	-	-	-
WES	74.10	311	IPC	25	-	-	-
YKC	77.40	344	EPC*	24	-	-	-
BAG	80.31	77	EPC	23	-	-	-
MAT	80.99	51	IPC	23	-	-	-
PPR	82.63	83	EPD*	22	-	-	-
TRT	88.10	101	IPD*	21	-	-	-
CGP	88.18	81	EPD*	21	-	-	-
MSO	91.13	337	IPC*	20	-	-	-

* : Phase determined from Earthquake Data Report (EDR)
\# : E(deg) = Observed S-wave polarization angle in degrees
$: Quality = Difference (Delta) between observed S-wave polarization angle and the theoretical S-wave polarization angle specified by the focal mechanism solution obtained.
Delta less than 20 degrees = Good
Delta between 20 and 25 degrees = Fair
Delta grater than 25 degrees = Poor

The vita has been removed from the scanned document

COMPUTER DERIVED FOCAL MECHANISMS FOR SELECTED EARTHQUAKES OFF THE SOUTH AND WEST COASTS OF TURKEY

by

T. Hakan Hazneci

(ABSTRACT)

Focal mechanisms of earthquakes, two of them in the Gulf of Antalya and one in the eastern Aegean Sea, were determined by using both P-wave polarities and S-wave polarization angles. Additionally, a focal mechanism solution for a third Gulf of Antalya earthquake was determined from P-wave polarities only. The polarity data were read from long period vertical (LPZ) seismograms of World Wide Standard Seismograph Network (WWSSN) stations. Additional polarity data were obtained from published earthquake listings. S-wave polarization angles were determined from particle motion diagrams for both the linear, and non-linear distance ranges. To determine polarization angles for the non-linear range stations, a correction technique developed by Nuttli (1964) was applied.

A revised version of the computer program written by Guinn (1977) was employed to obtain the focal mechanism solutions.

The focal mechanisms for the Gulf of Antalya events indicated strike-slip normal (28 May 1979 and 26 April 1981 events) and strike-slip thrust faulting (1 June 1977 event). All of the earthquakes occurred in this region are not far more than 50 kilometers from each other with focal depths ranging from 66 to 98 kilometers. The occurence of opposite type of faults in the Gulf of Antalya indicate a complex tectonics in that region.

Additionally, the focal mechanism of the Aegean Sea earthquake showed east-west striking normal faulting. The solution is in agreement with the focal mechanisms of the previous regional events (McKenzie, 1972 and Alptekin, 1973), indicating the continuation of the east-west oriented graben systems of western Turkey in the Aegean Sea.